



Review article

Planar MIMO antenna for mmWave applications: Evolution, present status & future scope

Parveez Shariff B. G^a, Pallavi R. Mane^a, Pradeep Kumar^b, Tanweer Ali^{a,*},
M. Gulam Nabi Alsath^c

^a Department of Electronics and Communication Engineering, Manipal Institute of Technology, Manipal Academy of Higher Education, Manipal 576104, India

^b Discipline of Electrical, Electronic and Computer Engineering, University of KwaZulu-Natal, Durban 4041, South Africa

^c Department of Electronics and Communication Engineering, Sri Sivasubramaniya Nadar College of Engineering, Kalavakkam, Chennai 603110, India

ARTICLE INFO

Keywords:

mmWave
MIMO antenna
Slot antenna
DGS
EBG-Based antenna
Vivaldi antenna
Metamaterial

ABSTRACT

The increased traffic in e-commerce, cloud-based processing, social media, and online video streaming demands higher data rates. The current 4G has reached the bottleneck, due to which it may not be able to fulfill the high data demand, so the focus is drifting toward millimeter wave (mmWave). The mmWave spectrum ranging from 30 to 300 GHz offers wide bandwidth with low latency, which finds its application in various communication fields, including 5G cellular. Despite its atmospheric attenuation and non-line-of-sight (NLOS) propagation, most countries are currently adopting mmWave 5G at the 28/38 GHz band due to less atmospheric attenuation, low path loss exponent, and low signal spread at these bands. The single-element patch antenna is a compact solution for mmWave applications, but its performance is inferior in terms of bandwidth, gain, and radiation efficiency. The array antennas have overcome these demerits, as it has shown a significant increase in bandwidth, gain, and radiation efficiency. Still, it has a limitation on data rate support. As a result, Multiple-Input-Multiple-Output (MIMO) technology can increase the data rate to 1000 times through spatial diversity and multiplexing techniques. So, to refine the performance further, there is a need to comprehend the MIMO antenna structures designed so far at mmWave. This paper presents the planar MIMO antenna structures developed so far, categorized here as slot, coplanar waveguide, defected ground structures, tapered/Vivaldi, meta-surface/metamaterial, dielectric resonator, and flexible antennas. The performance of these designs is compared based on bandwidth, gain, isolation, efficiency, and radiation pattern. This article also discusses the effects of slots, partial ground, and decoupling structures on impedance matching, bandwidth, and isolation levels. Also, a thorough discussion of the design issues and future work to be undertaken is discussed in this here.

1. Introduction

There has always been a hunger for a higher data rate, which imposes the challenge for network providers to provide customers with high mobile internet data. Nowadays, most of the applications are cloud or online-based, which demands uninterrupted, low

* Corresponding author.

E-mail address: tanweer.ali@manipal.edu (T. Ali).

latency, and high-speed data, which can be satisfied through 5G technology. Currently, various countries around the globe are establishing 5G technology to provide service to customers. In India, a 26 GHz band of mmWave for 5G has been rolled out recently by the Telecommunication Regulatory Authority of India (TRAI), and the services by vendors may begin soon [1,2].

The International Telecommunication Union (ITU) has approximated that 4.9 billion people of the world's population will be using the internet by 2021 [3]. This constitutes approximately 60% of the world's population. As of Dec 31, 2021, there are 5.2 billion people around the globe using the internet [4]. The statistics of average data consumption over the past decade and usage of the internet by various countries are shown in Figs. 1 and 2. Currently, 4G Long Term Evolution (LTE) has reached its saturation limit in data support due to its limited bandwidth and increased number of subscribers. The rollout of mmWave for 5G enhances the scope for a higher data rate due to its wide bandwidth despite its limitation. Most countries currently operate 5G at mmWave under Group 30 and 40 bands, as the World Radiocommunication Conference (WRC) recommended [5]. In Ref. [6], the authors proposed the strategies and policies to implement 5G for low and lower-middle-income countries based on the studies performed on countries that have already implemented 5G.

The mmWave opens the broad horizon to wireless communication technology by offering a wide bandwidth operating at the spectrum of 30–300 GHz [7]. The wavelength (λ) at the mmWave is about 1 mm (1–10 mm) which falls under the category of Extremely High Frequency (EHF) as per the International Telecommunication Union (ITU) standards.

Due to the higher wavelength and broad spectrum at mmWave, the Federal Communication Commission FCC has increased the minimum bandwidth to 400 MHz [9] compared to 4G (LTE), which has a maximum of 100 MHz bandwidth at 2300 MHz and 3300 MHz. The advantages of mmWave are shown in Fig. 3.

As mmWave has a high carrier frequency, the signal baud rate could carry more data, resulting in a high data rate (bits/sec/Hz) and reducing the buffering time in delivering high-quality videos [10]. The mmWave has a limited range, this help in cellular communication to expand the network coverage with the concept of frequency re-use through cell splitting and sectoring. The other applications of mmWave are in radar and image sensing [11,12], next-gen-Wifi (WiGig), Virtual reality for 3D rendering, medical applications [13,14], military applications [15,16], and IoT applications [17] as mentioned in Fig. 4.

Apart from the advantages mentioned above, there are certain downsides to mmWave, because it suffers from atmospheric attenuation due to gaseous losses (absorption of radio signals by water vapor and oxygen) and rain [18], and propagation path losses [19,20]. The mmWave signal experience atmospheric attenuation above 10 GHz due to hydrogen (H_2O) and oxygen (O_2) molecules. At 20 GHz, 200 GHz, and 250 GHz, the signal experience significant attenuation due to H_2O , and at 4 GHz and 100 GHz, attenuation is substantial due to O_2 . The mmWave also suffers from signal scattering due to a smaller wavelength than raindrops or foliage [21]. Another drawback of mmWave is that it mainly supports line-of-sight (LOS), due to smaller wavelength signal cannot penetrate through thicker objects/buildings [22–24]. The analysis of channel measurement in urban/suburban [9,25] areas for non-line-of-sight (NLOS) mmWave has shown low path loss exponent and signal spread, due to which it has found its prominence at 5G applications.

In a wireless communication system, the antenna plays a pivotal role in transmitting/receiving the signal with high gain and directivity. In the early stage of mmWave technology, a study [26] revealed the antenna gain enhancement technique through reflector design, lens, array, and horn techniques.

This paper presents a detailed discussion of MIMO antenna structures developed so far that supports the mmWave band. Therefore, understanding existing antennas structural behavior and performance help in solving the current issues. The key contribution of this article is as follows:

- It provides an overview of MIMO antennas at mmWave, and various methods to reduce the surface wave current and isolation enhancement techniques.
- Analysis of metamaterial structure used to enhance the antenna performance.
- It discusses the importance of slots, slits, and defective ground in designing antenna structures and their effect on antenna performance.
- It discusses the merits of current designs and challenges to improve the antenna structure for better performance of MIMO antennas.

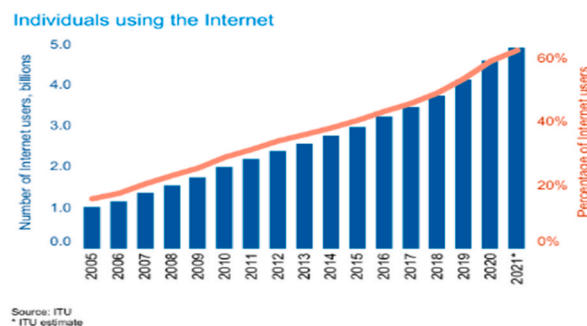


Fig. 1. Statistics of internet usage from ITU [3].

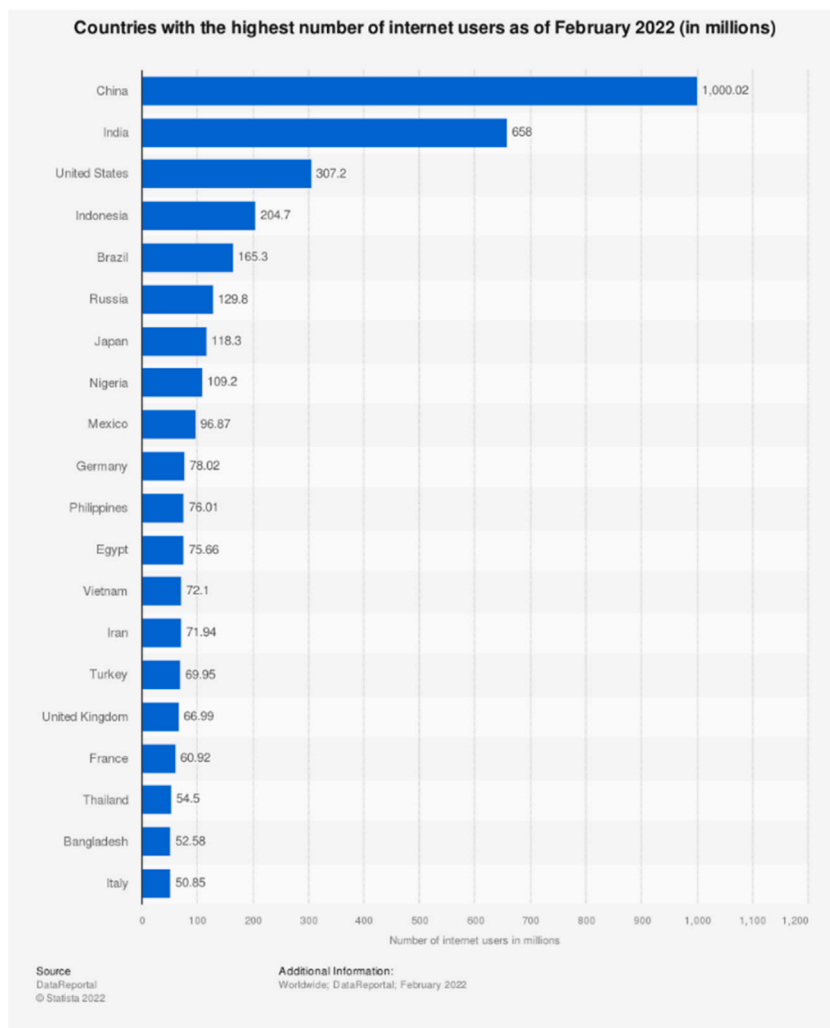


Fig. 2. Statistics of internet usage by various countries [8].

The organization of this paper is as follows: Section II introduces the types of antennas under the mmWave category. Section III presents the review of various MIMO antennas for mmWave, followed by a discussion, conclusion and future scope in sections IV and V.

2. Antennas for mmWave

The antenna technology plays a pivotal role in establishing communication. The most straightforward and compact mmWave antenna is the single-element antenna structure which can be planar [27–30], transparent [31], planar antenna with metamaterial loaded [30,32], tapered slot antenna [33,34], the bow-tie antenna [35] and so on. But the single-element structure performs poorly in terms of gain, bandwidth, and efficiency. Also, the radiation pattern is mostly omnidirectional, whereas the 5G mobile application requires a narrow beam directional radiation pattern.

Array antennas can overcome these issues [36] as it has many advantages, such as wide-angle beam scanning, adaptive beam-forming, multiple beams, wide bandwidth, and improved gain [37]. The design of a planar array requires proper spacing between the radiating elements in the x and y direction to reduce the side-lobe level and eliminate the grating lobes [38]. Usually, this spacing should be less than or equal to $\lambda/2$ [39]. For wide-beam scanning, radiating array elements are grouped in rows, columns, or areas called subarrays, which are fed separately through a phase shifter. Though the array antennas have improved the bandwidth, gain, and radiation performance compared to single-element antennas, there is no significant improvement in data rate. Hence this can be obtained through Multiple-Input-Multiple-Output (MIMO) antennas at the mmWave band [40]. The discussion of array antennas is out of scope in this article as these antennas are categories based on feeding techniques [41–44] and reconfigurability [45–47]. Hence, the focus of this review article is restricted to planar MIMO antennas because these antennas perform better in terms of gain, bandwidth, directivity, and data rate. Also, these antennas are low profile and easy to implement at 5G handsets. We have categorized the MIMO antennas based on design structure, as indicated in Fig. 5 Section III discusses various planar MIMO antennas' performance and design

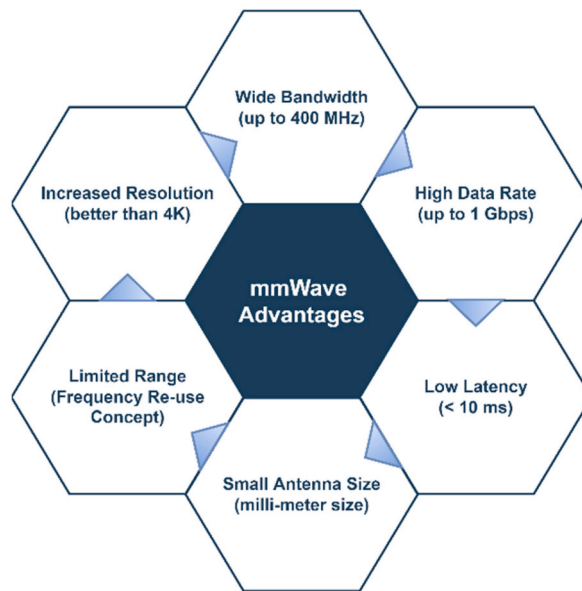


Fig. 3. Advantages of mmWave.

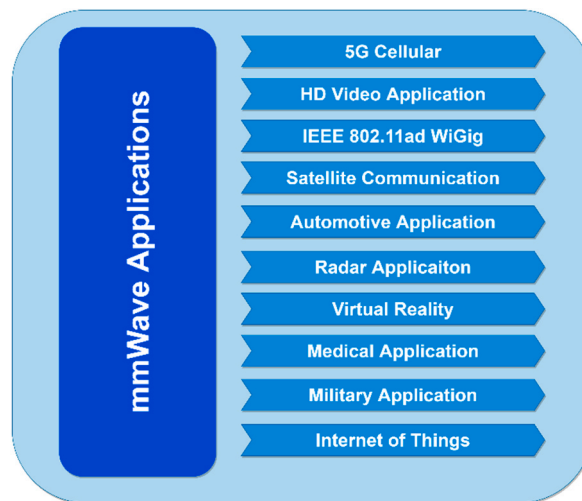


Fig. 4. Applications of mmWave.

structure.

The MIMO antennas are very useful in dense environments where LOS communication is impossible. In such cases, the signal arriving at the receiver through multipath may be in-phase or out-of-phase, resulting in multipath fading [48]. This multipath issue is mitigated by the MIMO antenna, which is connected to a combiner to get a higher mean signal-to-noise (SNR) ratio resulting in diversity gain as shown in Fig. 6. There are four diversity combiners: selection combining, switched, equal gain combining (EGC), and maximum ratio combining (MRC). In selection combining, the branch with high SNR is selected at any point in time. Switched combiner selects the signal from the branch which satisfies the minimum threshold value. EGC adds the co-phased branch signals. In MRC, the phase weights are applied to each branch such that the output will be the sum of their SNR ratios [49,50].

Initially, MIMO antennas are used to increase spatial diversity to counter channel fading. It is considering Rayleigh fading environment, where the information is transmitted through m antennas which follow multiple paths to reach the multiple n receiving antenna independently. In this case, the maximum diversity gain is mn , which is termed *Spatial Diversity*. In another scenario, when independent information is transmitted through m antennas, the data rate is increased, which is referred to as *Spatial Multiplexing* [51, 52]. In Ref. [53], the non-asymptotic approach determines the practical number of transmit antennas required to increase the channel capacity.

In a MIMO system, mutual coupling loss and correlation coefficient between the antennas must be low. The mutual coupling loss

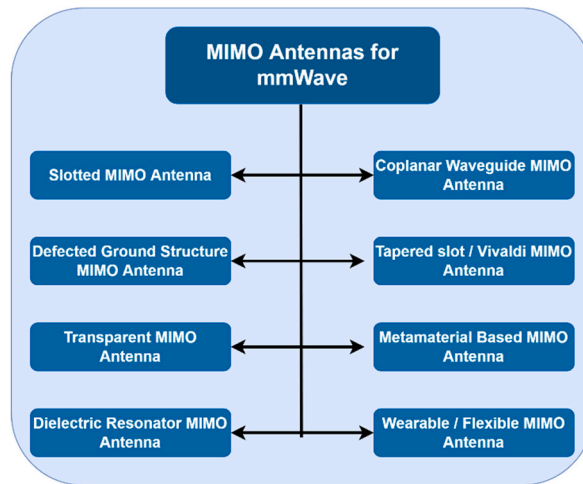


Fig. 5. Types of MIMO antenna for mmWave.

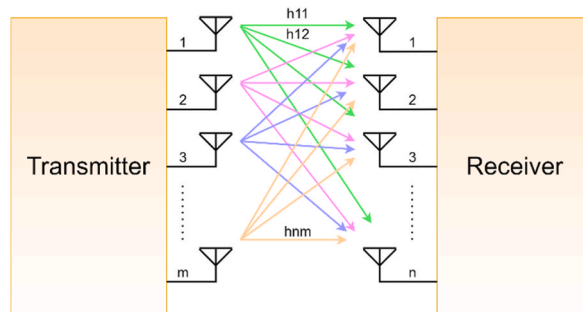


Fig. 6. General overview of MIMO.

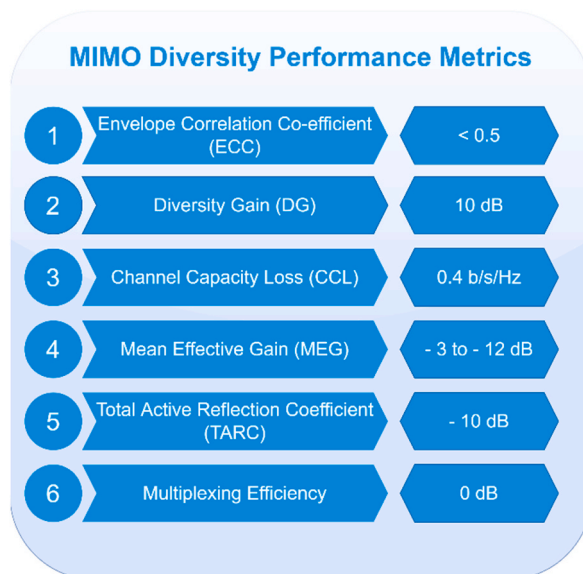


Fig. 7. MIMO diversity parameter metrics.

gets significant when the antenna spacing $d < 0.2\lambda$ for $M \leq 4$, where M is the number of antennas and λ is the operating frequency [54]. The performance of the MIMO antennas is validated through the diversity parameters metrics as presented in Fig. 7. These are Envelope Correlation Coefficient (ECC), Diversity Gain (DG), Channel Capacity Loss (CCL), Mean Effective Gain (MEG), Total Active Reflection Coefficient (TARC), and Multiplexing Efficiency. The equations and the minimum threshold value of these parameters are specified in Refs. [55–58].

The 3rd Generation Partnership Project (3GPP) has issued the enhanced standards for MIMO antennas for 5G in its release-17 [59], which is summarized in Fig. 8. The focus of 3GPP as follows: to emphasize the massive enhancement of MIMO transmission and reception quality, multi-beam formation, support for non-terrestrial coverage at sub-7 GHz, reduced power consumption by antenna tuning system in mobiles such that power consumption on mobile is low, spectrum expansion from 24.25 to 52.6 GHz up to 71 GHz, reduced bandwidth support for lower complex IoT devices at 20 MHz/100 MHz in new sub-7/mmWave, mobile MIMO antennas to support direct satellite communication, support for GNSS positioning system and support standalone broadcast at 6/7/8 MHz carrier bandwidth.

3. MIMO antenna for mmWave applications

Various types of antennas are designed for mmWave applications that use MIMO technology. In this article, MIMO antennas are categorized based on the structural design as a slot antenna, coplanar waveguide antenna (CPW), defected ground antenna, tapered/Vivaldi antenna, transparent antenna, meta-surface/metamaterial-based antenna, dielectric resonator antenna (DRA), and flexible antenna, as shown in Fig. 5. Here, MIMO antennas are analyzed based on design, bandwidth at reflection coefficient $S_{ii} < -10$ dB (where i is the exciting port), isolation level S_{ij} (where i and j are not equal), gain, efficiency, and radiation pattern at half-power-beamwidth (HPBW).

3.1. Slot MIMO antenna

Most planar microstrip antennas are designed using a single substrate, making them cost-efficient with reduced complexity. In planar antennas, slots [53] are introduced to obtain multi-band resonance, improve bandwidth, and reduce surface wave or coupling losses. The most common types of slots are E – shape [60], U – shape [61], and fractal-shape [62] slots in the radiating plane. The input port of radiating element should match the 50 Ω microstrip feed line (which depends on the width) for maximum power coupling to obtain maximum radiation efficiency. This section discusses various slot MIMO antennas.

The antennas proposed in Refs. [63,64] share the same plane to design the two different types of antenna structure to resonate at



Fig. 8. 3GPP standards for 5G MIMO antennas release –17.

sub-6 GHz and mmWave, whereas in Ref. [65] single antenna type structure is designed to resonate at multiple bands, which is fed by two different feeds. In Ref. [63], Rogers 5880 substrate is used, where the ground plane is etched with a T-shaped open-ended slot fed by a transmission line of L-shape and meander branch to resonate at 1.6–2.2 GHz. Another open-ended inverted L-shaped slot is etched on the ground plane to resonate at 3.3–5 GHz with a horizontal stub at the center to improve the bandwidth. And to obtain resonance at mmWave frequency 27–29 GHz, an open-ended rectangular slot is etched on the ground plane with a tilt to the right side. Due to this, current flow in the anti-clockwise direction with an increase in phase resulting in right-handed circular polarization. In Ref. [64], Rogers RO4350B is chosen on which a Y-shaped antenna is etched on top to resonate at 5.29–6.26 GHz. A circular slot is etched on the bottom of the ground plane underneath the radiating element to improve the radiation performance. For the mmWave band, a rectangular patch is slotted in C-shape and extended to a two-element array connected to a T-junction parallel feed. The isolation between the two elements is improved by introducing the rectangular slot in the ground plane and the circular slot to improve the radiation performance.

In [65], the design has four hexagonal shape slots in the ground plane, which are fed by two separate feeds to resonate at different frequencies placed on the other side of the RO4350 substrate. The open-ended 50 Ω transmission line resonates at sub-6 GHz, whereas a standard 1 × 8 power divider (PD) feed is used to excite at mmWave. The spacing between the PD is maintained at λ₀/2 (where λ₀ is the lowest resonating frequency in this article) to provide better isolation between the feed arms. One hexagonal slot is carved with three other inner hexagonal shapes to obtain the multi-band resonance at sub-6 GHz. The parametric study is performed to tune the length of the open-end transmission line and PD. At mmWave, the surface area near to outer hexagonal slot is a radiating element, as most of the current distribution is near it.

The single-element designs of [63,64], and [65] are extended to 16-port, 4-port, and 2-port MIMO. The performance metrics of these in terms of gain, bandwidth at reflection S_{ii} < -10 dB, isolation S_{ij}, and radiation at HPBW are 12 dBi, 9.53 dBi, 7.6 dBi, 27–29 GHz, 26–29.5 GHz, 27.7–28.3 GHz, -20 dB, -22 dB, -28 dB, and 10⁰ RHCP [63], broadside radiation with HPBW of 80⁰ & 50⁰ in E- and H-plane [64], omnidirectional. All these antennas are designed on a large substrate where MIMO port spacing is large, resulting in better isolation [65].

The designed structures are compact in Refs. [66,67], and [68], resonating at 28 GHz/29 GHz/38 GHz with 2-port and 4-port MIMO. The S-shape design in Ref. [66] with an inter-element spacing of 0.41λ₀. The single element is a rectangular patch etched on top of the FR4 substrate, which is fed by a 50Ω microstrip line, the bottom of the substrate has a full ground plane. The design is optimized by introducing a horizontal slit on the right of the patch head, which forms an L-shaped slot. Due to this, the resonance has drifted to a slightly higher frequency. Another slit on the left bottom of the patch forms the L-shaped slit to improve the impedance matching. With this, a better reflection coefficient S_{ii} of -30 dB is obtained. This design is expanded to 2-port MIMO by placing the radiating elements in symmetry and asymmetry form. Both arrangements are studied to understand the surface current distribution and mutual coupling. The maximum current is concentrated near the slits, which reduces the mutual coupling in the asymmetrical orientation of antennas, making the structure compact and avoiding using a decoupling structure.

Another 2-port, compact rectangular patch with 45⁰ tilt is designed to obtain a higher isolation S_{ij} in Ref. [67]. The design is etched on Rogers 4350B substrate. The 50 Ω microstrip feed is connected offset to the left of the rectangular patch. The isolation was -16 dB when the two patches were straight, which is improved by inserting a slit at the top and bottom of the patch and tilting the patch by 45⁰. Due to this modification, the current path has increased, resulting in improved isolation of -36 dB, and resonance is dropped to 29 GHz from 36 GHz. The design in Ref. [68] resulted in high gain and better bandwidth. Here, the monopole antenna is an arc-shaped stripe obtained from the evolution of the circular patches. This design has 4-arcs of varied lengths etched on top of the Rogers 5880 substrate. Four such elements are orthogonally aligned to reduce the mutual coupling.

The performance metrics of the above designs are as follows: bandwidth 28–28.6 GHz, 28.8–29.7 GHz, and 24–39 GHz, gain 5.8 dBi, 6 dBi, and 10.5 dBi, isolation -30 dB, -25 dB, and -20 dB, and radiation omnidirectional [66], broadside with HPBW of 40⁰ and 30⁰ in E- and H-plane [67], and broadside with HPBW of 60⁰ in E- and H-plane [68]. The performance metrics of slot MIMO antennas are shown in Figs. 9–11. The prototype fabrications are shown in Fig. 12(a–f).

3.2. Coplanar waveguide MIMO antenna

Another way to reduce transmission line losses, surface wave, and substrate losses is with a coplanar waveguide (CPW) antenna [69]. A few planar antennas designed with the concept of CPW/grounded-CPW are [70–73], in which the first two designs don't share

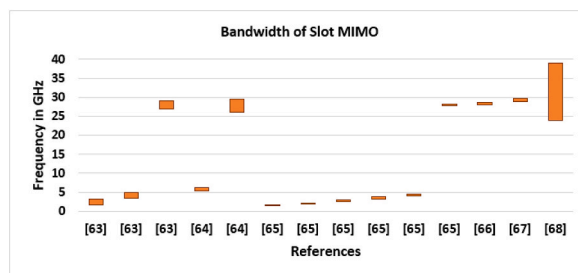


Fig. 9. Performance metrics in terms of bandwidth of slot MIMO antennas.

antenna to obtain the desired bandwidth of 26.5–30 GHz. The power is fed by a 50 Ω microstrip line, which uses a grounded coplanar waveguide (GCPW) technique, in which a grounded patch surrounds the transmission line. The feeding point to radiating element is connected at an offset from the center towards the left to increase the current flow, which could result in end-fire radiation. In Ref. [71], 2-port MIMO is designed, which has a T-shaped patch as radiating element on top of the Rogers 5880 substrate. The radiating element is fed by a 50 Ω microstrip line supported with grounded CPW. The antenna is optimized by trimming the edges of the T-shape patch and CPW. Two rectangular slots of square split ring resonators are etched on CPW in a complementary fashion, improving the impedance bandwidth and gain. The ground plane is optimized to the partial ground with circular split rings, resulting in better impedance bandwidth at 26.8–37.8 GHz. The performance of these designs are bandwidth 26.25–30.14 GHz and 26.5–32.7 GHz/35–38.4 GHz, gain 5.8 dBi, and 6.4/5 dBi, isolation –30 dB and –13/–24 dB, and radiation is end-fire at 100⁰ with HPBW of 65⁰ in E- and H-plane [70], and omnidirectional in Ref. [71].

3.2.2. Common ground

A compact, sickle shape, 4 – port MIMO antenna is proposed in Ref. [72] to resonate at wide bandwidth from 1.3 to 40 GHz. The initial design is a monopole antenna of sickle shape on either side of the ground plane, which is fed by a coplanar waveguide (CPW). Further, the sickle shape is modified to a self-complementary structure to enhance the bandwidth, and this is done by extending the ground plane vertically and etching the left side of the sickle shape.

Next, the feed line is modified to tapered feed, and the right side of the ground is extended. In this design, three notch filters are added to introduce stopband at 2.4 GHz (Bluetooth), 5.5 GHz (WLAN), and 7.5 GHz (X-band). It is achieved by inserting two split ring resonators (SRR) [74–76] and an L-shaped slit in the radiator. The magnetic resonance, Q-factor, split width, gap, metal width, and capacitance effect of SRR are studied in Refs. [74,76]. The two SRRs reject 5.5 and 7.5 GHz, whereas the L-shape slit rejects 2.4 GHz. The comprehension from the current distribution reveals that at 2.4 GHz, the maximum current is at the L-shaped slit. Likewise, at 5.5 GHz and 7.5 GHz, the maximum current is at the outer SSR and inner SSR. The single-element is extended to a 4-port MIMO with orthogonal orientation for better isolation. The ground plane of all the ports is connected to a circular ring at the center for better isolation.

In [73], the design has a circular patch with an elliptical slot at the center, and two parasitic elements of a small circular patch on either side of the feed line, which acts as CPW, etched on top of Rogers 5880 substrate. The radius of the circular patch, parasitic element, elliptical slot, and the ground plane is varied to get the optimum wide bandwidth. The design is extended to a 4-port MIMO by placing the antennas orthogonal to each other for better isolation. Due to the interconnection of the ring, a small amount of coupling current can be seen at 26, 30, 32, 36, and 40 GHz. The performance of these MIMO antennas is as follows: bandwidth 1.3–40 GHz and 24.8–44.45 GHz, gain 6 dBi and 5.68 dBi, isolation –25 dB and –20 dB, and radiation is omnidirectional in Refs. [72,73]. The performance metrics of CPW MIMO antennas are shown in Figs. 13 and 14. The design/prototype fabrication of these CPW MIMO antennas is shown in Fig. 15(a–d).

3.3. Defected ground structure MIMO antenna

In planar microstrip antennas, the ground plane acts as a reflector, due to which the radiation will be normal to the radiating element. But to improve the antenna bandwidth or to obtain better isolation between elements, the ground plane can be optimized from full ground to partial ground, called defected ground plane structures (DGS). Such structures compromise the directivity of the radiation pattern. The DGS can be of any geometric shape such as rectangle, circular, E, H, I, or ring shape [77] etched on the ground to enhance the desired parameter. In this subsection, we will discuss MIMO antennas that share and do not share the common ground of DGS structures.

3.3.1. Non-common ground

The MIMO antennas designed in Refs. [56,78–86] don't share the common ground point, which obviously results in better isolation S_{ij} between the ports. And also, these are arranged in 180⁰/orthogonal orientation to reduce mutual coupling and enhance isolation. The 2-port MIMO in Ref. [78] is designed to resonate at 27 and 39 GHz, placed in 180⁰ orientation. Here, a single element is a square patch with an extended stub along the width to increase the current density over the partial ground plane, resulting in resonance at 31 GHz. The second resonance is obtained by etching the rectangular slot in the radiator, which resonated at 27 GHz. In Ref. [79], two elements are placed orthogonal to each other. In this case, the single-element design is a rectangular patch that resonates at 28 GHz.

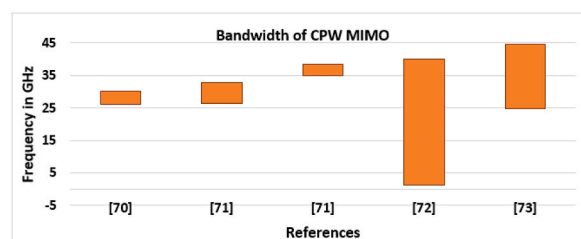


Fig. 13. Performance metrics in terms of bandwidth of CPW MIMO antennas.

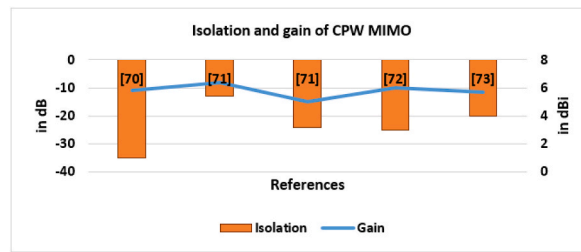


Fig. 14. Performance metrics in terms of isolation and gain of CPW MIMO antennas.

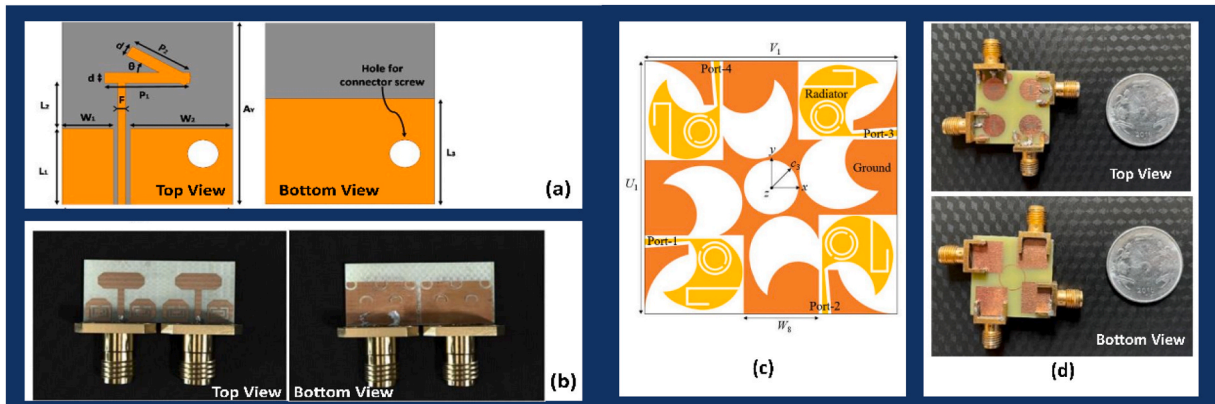


Fig. 15. Design/prototype fabrication of CPW MIMO antennas, (a) [70], (b) [71], (c) [72], and (d) [73].

The rectangular patch is etched to a hemispherical contour shape to resonate at 38 GHz. Further, the protrusion stub is added at the top of the element with a slit in the partial ground plane to improve the impedance. Both the designs [78,79] used Rogers 5880 substrate and fed by 50Ω microstrip line. The performance of these designs in terms of bandwidth, gain, isolation, and radiation pattern are: 25–28.2/36.2–41 GHz and 26.65–29.2/36.95–39.05 GHz, 5/5.7 dBi [78] and 1.27/1.83 dBi [79], –30 dB/–25 dB and –20 dB, and bidirectional/omnidirectional in E– and H-plane.

The MIMO design in Refs. [80–86], and [56] are the 4-port element which is orthogonal/180° oriented for better isolation with the partial ground plane. In Ref. [80], the design has two concentric circular rings on either side of the 50 Ω microstrip line. The small ring connects these concentric circles, forming an infinite shape shell. The semi-circular ring is added to the head of the ground to fine-tune the resonant frequency at 28 GHz. The design in Ref. [81] has a rectangular patch on Rogers 5880 with an inset feed that resonated at 28 GHz. An H-shape slot is etched on the radiator to enable resonance at 38 GHz. The 50 Ω microstrip line is optimized to the quarter-wave transformer to improve the impedance matching. The element in Ref. [82] has a circular patch on Rogers 5880 substrate fed by a 50 Ω microstrip line. Five circular pedals are connected via a strip line for a circular patch. An angle of 45 deg separates the circular pedals, and the ground plane is optimized to the partial ground to obtain the desired bandwidth. To tune the resonance frequency stub of the semi-circular ring is added to the ground plane. In Ref. [83], a rectangular patch is designed on Rogers 5880 substrate to resonate at 28 GHz with an inset feed quarter-wave transformer. A horizontal I-shaped slot is etched on the rectangular patch to resonate at 38 GHz. The ground plane is optimized to the partial ground to improve the bandwidth with a rectangular slit in the center to improve the isolation between elements. In this design, pair of elements share ground, but two pairs don't. An ample space separates the two pairs of elements with 180° orientation. Similar to the earlier design, a combination of T with a plow-shape structure is designed on Rogers 5880 substrate in Ref. [84]. The patch radiator is supported by a partial ground plane etched at the substrate's bottom to obtain the desired bandwidth. The square slit in the ground plane aided in obtaining the desired resonance. A 50 Ω microstrip line feeds the radiator. The plow-shape has an extended stub inverted inside at an angle of 15° for better resonance and wide bandwidth. A structure is fine-tuned after the parametric study on plow-shape angle and length and on T-shape structure. Further, the design is extended to 4-port MIMO, which is arranged orthogonally to maintain low surface wave coupling. In another design, a circular patch is etched on top of the Rogers 5880 substrate [85]. The better resonance at 28 GHz is obtained by introducing an elliptical slot in the radiator and trimming the sides of the ground plane. The design is extended to 2-port and then to 4-port MIMO. The radiating elements are arranged orthogonal to each other for better isolation.

In the next design, a line resonator of a fan-shaped decoupling structure is etched on top of the Rogers 5880 substrate to enhance the isolation [86]. The single-element is designed in three-stages, with the initial design of an I-shape radiator fed by a 50 Ω microstrip line. It resonated at 39 GHz. Next, the design is expanded to an inverted L-shape and then to a 90°-oriented S-shape structure, resulting in the desired response. Further, four elements are arranged orthogonally to each other, forming a 4-port MIMO. The decoupling

structure has four arms connected to a 45°-oriented square patch on top of the substrate. The line resonator decoupling structure has maximum isolation S_{ij} of -55 dB, greater than the structure without decoupling has -40 dB.

Similar to the earlier design, a modified line resonator of a fan-shaped decoupling structure is etched on the top and bottom of the Rogers 5880 substrate [56]. The single element is an elliptical patch with a 50Ω feed line, this created resonance at 33 GHz and 43 GHz. A rectangular slot underneath the patch has drifted the lower resonance to 28 GHz and higher to 44 GHz. The resonance has improved with better bandwidth at 28 GHz and 38 GHz with the inset feed technique. The design is extended to a 4-port MIMO with an orthogonal arrangement. The surface current is reduced further by carving a decoupling structure of four arms connected to a square patch. It has increased the isolation of -30 dB and higher throughout the band. The performance of these MIMO antennas is as follows: bandwidth 27.6–29.7 GHz, 27.6–28.4 GHz/37.9–38.5 GHz, 26–29 GHz, 27–28 GHz/37.2–38.8 GHz, 23.6–31.5 GHz, 26.5–30.8 GHz, 24.2–37.8 GHz, and 27–28.8 GHz/36–38.7 GHz, gain 6.1 dBi, 7.9 dBi, 6.5 dBi, 7.95/8.27 dBi, 5.66 dBi, 8 dBi, 6.4 dBi, 6 dBi/5 dBi, isolation -29 dB, -28 dB, -25 dB, $-30/-24$ dB, -27.5 dB, -22.5 dB, -27 dB, -30 dB/ -32.5 dB and radiation is omnidirectional [80], broadside with 35° in E- and H-plane [81], omnidirectional [82], broadside with 60° at 28 GHz, 90° at 38 GHz in E-plane [83], omnidirectional [84], bidirectional with 110° in E-plane [85], bidirectional with 60° and 70° in E- and H-plane [86], 75° and 90° in E- and H-plane at 28 GHz/ 90° in E- and H-plane at 38 GHz [56]. The performance metrics of DGS non-common ground MIMO antennas are shown in Figs. 16–18. The prototype fabrication is shown in Fig. 19(a–j).

3.3.2. Common ground

In [55,87–94], and [95], the designs share the common ground between all ports of MIMO, in which the first four are 2-port, and others are 4-port MIMO where elements are arranged in orthogonal orientation for better isolation. In Ref. [87], the antenna is developed in two phases: in phase one, a rectangular patch is etched on top of the Rogers 4003 substrate. In phase two, a rectangular slit is etched on the radiator, which appears to be a U-shape with a rectangular slot in the ground plane underneath the radiator. Due to phase two modification, the resonance is shifted from 50 GHz to 26.5 GHz. The parametric study on the slit, slot length, and width is performed to fine-tune the resonance and improve the bandwidth. This structure has resulted in a bandwidth of 26.5–32.9 GHz.

In [88], an ultra-wideband antenna is designed with a decoupling structure. The single radiating element is a combination of a rectangular patch and semi-circle, which is fed by a 50Ω microstrip line etched on top of the FR4 substrate. The ground plane is defected to the partial ground to attain the wide bandwidth. But due to the proximity of two radiating elements, induced mutual coupling caused by the surface current degrades the MIMO diversity parameters. For this reason, the design is upgraded with a decoupling stub of I-shape between the two radiating elements in the ground plane. After the parametric study, an elliptical strip was added to the decoupling structure's head, further improving the isolation. Both these designs are 2-port MIMO placed symmetrically to each other. Another compact 2-port MIMO with wide bandwidth is designed in Ref. [89]. The design is evolved in three stages, with the initial design of head trimmed circular patch etched on Rogers RO-4360B. The ground plane is trimmed to partial ground. Another circular patch with a trimmed head was added in the second stage, which improved the bandwidth. In the last stage, the cone structure is etched on top of the radiator, which results in a wide bandwidth. The optimum distance between MIMO resulted in a maximum of -30 dB. A dielectric layer of $20 \text{ mm} \times 26 \text{ mm}$ backs the design at a distance of 4 mm to improve the radiation performance. Similar to Ref. [88], an inverted L-shape decoupling structure is etched on the ground plane in Ref. [90]. The single-element is a 4-spoke wheel shape patch etched on top of the FR4 substrate. The partial ground plane is etched at the bottom of the substrate to improve the bandwidth and multiple resonances. With 12-spoke optimization in the radiator, the antenna resonated at five frequencies. The design is expanded to 2-port MIMO with an asymmetrical ground plane arrangement. The top center of the ground plane is optimized with a comb-like structure to reduce surface waves and increase isolation. It has improved the isolation to -26 dB.

The next design extends the two-element array to a 4-port MIMO [91]. Here a single element is a rectangular patch on top of the Rogers 5880 substrate. The element is modified with a circular slot at the center and semi-circular slits on four sides. A protrusion stub is added to improve the impedance at the head of the element. The design is extended to two element array fed by the parallel feed of the T-junction to distribute power with equal magnitude and phase. The spacing between array elements is crucial because it gives rise to high side-lobe levels and grating lobes if the spacing is less or more. The design is extended to 4-port MIMO, where the substrate is carved with a cross shape to reduce the mutual coupling. The dual-band resonance at 38 GHz is obtained by etching a circular slot in the ground plane. This design resulted in a good gain of 7.9 dBi and 13.7 dBi at 28 GHz and 38 GHz.

In [55], a two-element array is extended to a 4-port MIMO. Here, a single element is a rectangular patch on Rogers RO4350B. It is etched with an inverted C-shape slot and a slit at the left. Two such elements are separated by λ_0 distance, fed by a T-junction power

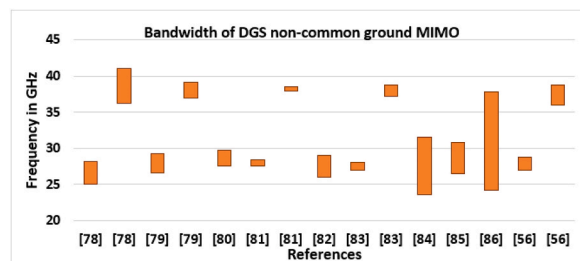


Fig. 16. Performance metrics in terms of bandwidth of DGS non-common ground MIMO antennas.

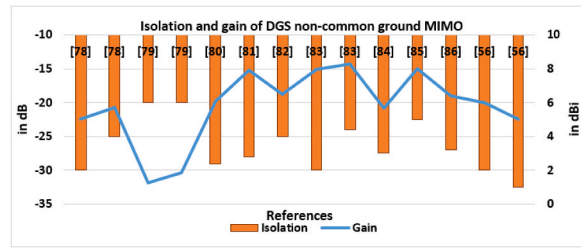


Fig. 17. Performance metrics in terms of isolation and gain of DGS non-common ground MIMO antennas.

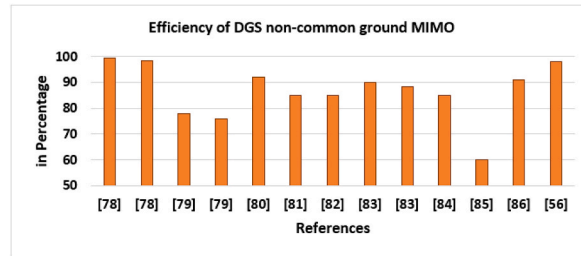


Fig. 18. Performance metrics in terms of efficiency of DGS non-common ground MIMO antennas.

divider. The current coupling between two elements is controlled by etching rectangular in the ground plane and a circular slot to improve the bandwidth. A zig-zag slot is etched in the center of the ground plane to reduce the coupling effect between MIMO ports. Another compact design with 4-port MIMO with increased isolation is proposed in Ref. [92]. In this design, the rectangular patch is modified in 4-stages to attain a shape of H-P, which could able to attain the desired band. The rectangular patch is etched on Rogers 5880 with offset feed, which has five slits on either side of the patch, which results in H-P shape. The single-element is extended to 4-port MIMO, whereas the substrate is trimmed with a z-shape to reduce current coupling between ports is reduced.

In [93], an inverted L-shape strip line is used as a decoupling structure to increase the isolation. The design has 4-port and 8-port MIMO, where each single element design is a circular arc on top of the FR4 substrate, obtained by subtracting two circles with partial overlapped. The ground plane has defected to the partial ground with an extended stub of an inverted L-shape and the semi-circular slit at the center of the ground plane. The design is optimized by varying the diameter of circles, the overlap of circles, and the length of the ground plane. The single-element is extended to 4 – port MIMO, where radiating elements are positioned orthogonally on plus shape substrate. The grounds of MIMO are connected through a microstrip line crossing at the center of the substrate. The same concept is extended to 8 – port MIMO.

Similar to the [55] design, a two-element, 4-port MIMO is proposed in Ref. [94]. A single element is a rectangular patch on Rogers 5880 substrate fed by a quarter-wave transformer. The current path is increased by introducing bow-tie slots at the center and rectangular slits at all sides of the patch. This resulted in drifting the resonance to the lower value of 28 GHz. The gain is increased by extending the design to a two-element array fed by parallel feed. Further, the structure is enhanced to a 4-port MIMO. Etching rectangular slits in the ground plane and zig-zag decoupling structure on the top layer, isolation has been increased to -40 dB.

Another 4-port MIMO structure is proposed in Ref. [95], with an inverted L-shape patch on Rogers 5880 substrate. The ground plane is reduced to partial ground to obtain the improved bandwidth. The design is extended to 3-port MIMO arranged orthogonal to each other. The rectangular slits between elements in the ground plane have increased the isolation S_{ij} to -20 dB. Further, the 4-port MIMO is designed where elements are orthogonal to each other. The ground planes of all ports are connected through a circular ring to maintain the constant reference voltage. The performance metrics of these designs are as follows: bandwidth 26.5–32.9 GHz, 3–40 GHz, 17–25 GHz, 1–4 GHz/5.5–6.8 GHz/9.5–10 GHz/12–13.5 GHz/14.8–16 GHz, 27.5–28.9/37.2–38.5 GHz, 25.5–29.6 GHz, 37–40 GHz, 2.84–11 GHz, 27.5–28.5 GHz, 27.4–40 GHz, gain 5 dBi, 6 dBi, 6.5 dBi, 3 dBi/4.8 dBi, 7.9 dBi/13.7 dBi, 8.3 dBi, 6.5 dBi, 5.6 dBi, 11 dBi, 9 dBi, isolation -35 dB, -20 dB, -16 dB, -27 dB, -25 dB, -17 dB, -25 dB, -15 dB, -38 dB, -30 dB and radiation broadside with 90° and 60° in E– and H-plane [87], omnidirectional [88], bidirectional with HPBW of 70° in E– and H-plane [89], bidirectional [90], omnidirectional [91], broadside with 70° and 55° in E– and H-plane [55], 120° and 60° in E– and H-plane [92], 60° in E-plane [93], and broadside with 40° and 50° in E– and H-plane [94], omnidirectional [95]. The performance metrics are shown in Figs. 20–22. The prototype fabrication of DGS common ground designs is shown in Fig. 23(a–j).

3.4. Tapered/Vivaldi antenna

The tapered slot antennas are also called Vivaldi antennas. The tapered slot antenna can be exploited to achieve dual functions. It works as a decoupling structure at a lower frequency with a length of $\lambda_0/2$ and acts as a tapered antenna of $3\lambda_0$ long at a higher frequency. The theoretical modeling of taper shape and electric-field distribution is studied in Ref. [96].

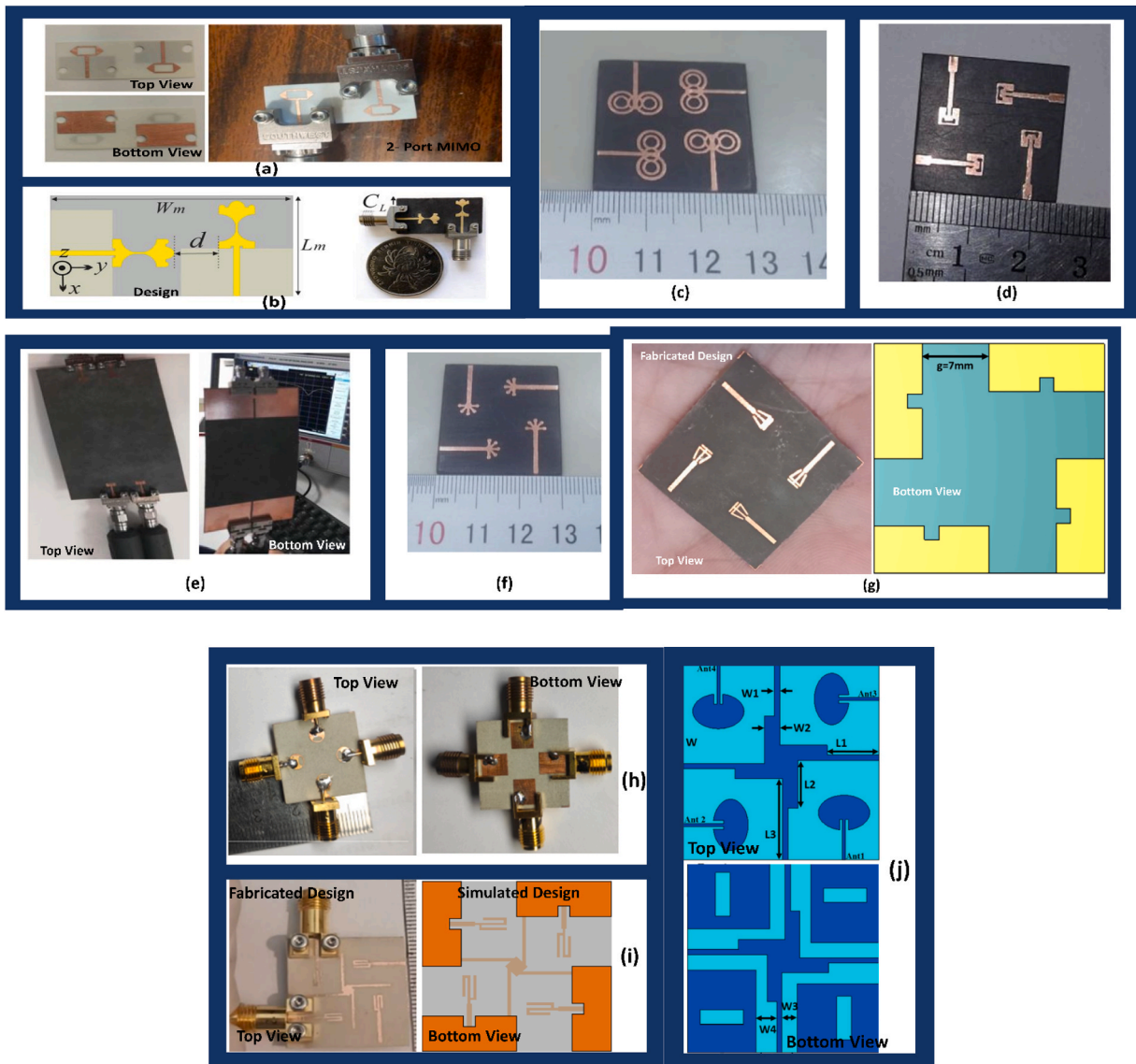


Fig. 19. Prototype fabrication of DGS non-common ground MIMO antennas, (a) [78], (b) [79], (c) [80], (d) [81], (e) [83], (f) [82], (g) [84], (h) [85], (i) [86], (j) [56].

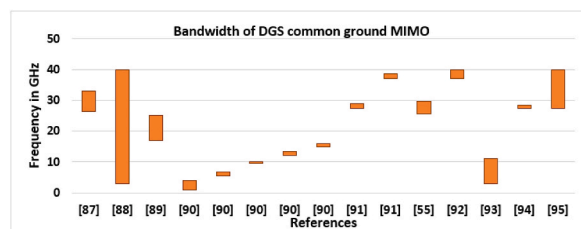


Fig. 20. Performance metrics in terms of bandwidth of DGS with common ground MIMO antennas.

Here [97,98] are tapered/Vivaldi antennas used to resonate at sub-6 GHz and mmWave band. In Ref. [97], a Rogers 5880 square substrate is used, on which a monopole antenna is etched on top with a ground plane at the bottom. The substrate's edges are trimmed, and the ground plane has a circular slot at the center with a rectangle slot at the corners. The four sub-6 GHz monopole antennas are extended from the side of the square substrate to the center, each with two arms. Likewise, four L-shape microstrip lines terminated

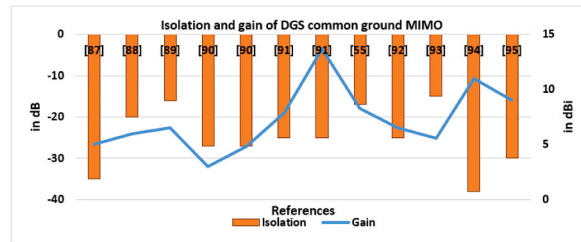


Fig. 21. Performance metrics in terms of isolation and gain of DGS with common ground MIMO antennas.

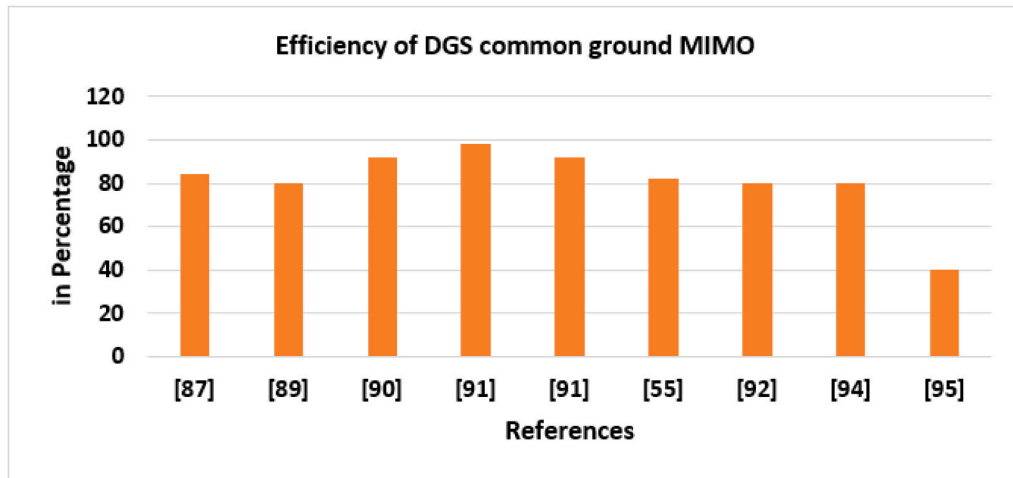


Fig. 22. Performance metrics in terms of efficiency of DGS with common ground MIMO antennas.

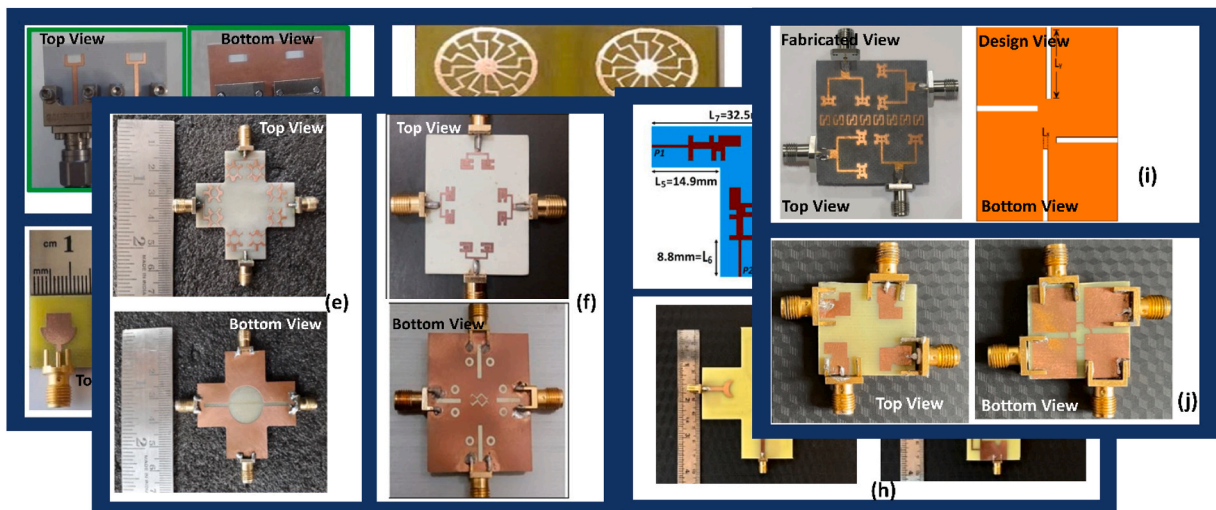


Fig. 23. Prototype fabrication of DGS common ground MIMO antennas, (a) [87], (b) [88], (c) [89], (d) [90], (e) [91], (f) [55], (g) [92], (h) [93], (i) [94], (j) [95].

with circular stubs for impedance matching at mmWave are etched at the vertices of the substrate. When sub-6 GHz antenna-1 is excited, the current between antenna-1 and antenna-2 is coupled through the edges of the ground plane slot. The insertion of the slot between the two antennas in the ground plane reduces the mutual coupling, as this acts as a stopband filter. But this has resulted in a drift of resonance to a higher frequency due to vertex slots. The vertex slot behaves like a stop band filter and improves the isolation at sub-6 GHz. The rectangular slot is modified to a tapered slot, which is also used as a wideband antenna for mmWave. The operating

frequency at mmWave and sub-6 GHz are largely separated, due to which resonance at 28 GHz and band-stop filter at 2.45 GHz are independent of each other.

Similar to the earlier design [98], uses Rogers 5880 substrate with a rectangular slot of varied width in the ground plane, which is excited by monopole antennas of sub-6 GHz and mmWave, etched on top of the substrate. The monopole antenna of mmWave is terminated with a circular stub for better impedance matching, which excites the tip of the tapered slot to resonate from 25 to 40 GHz. The monopole antenna of sub-6 GHz is placed horizontally at the center of the tapered slot. It excites to resonate at 2 GHz, acting as an open-ended slot antenna. But the issue is that most of the mmWave power is trapped around the sub-6 GHz feeder, which behaves like shunt impedance. This issue is addressed by optimizing the thickness of the sub-6 GHz feed line at the slot and introducing a low pass filter (LPF) to improve the isolation. The performance metrics of [97,98] are as follows: bandwidth 2.45–2.75 GHz/5.3–5.7 GHz/24–28 GHz and 1.9–2.3 GHz/26–33 GHz/37–40 GHz, gain 5 dBi/11 dBi and 3 dBi/6.2 dBi, isolation –16 dB/-23 dB and –15 dB/-25 dB, and radiation is broadside directional (tilt by 90° and 45° in E- and H-plane) with HPBW of 40° in E- and H-plane [97], and omnidirectional at sub-6 GHz/broadside with HPBW of 60° in E- and H-plane [98]. The performance metrics of tapered/Vivaldi MIMO antennas are shown in Figs. 24–26. The design/prototype fabrication is shown in Fig. 27(a and b).

3.5. Transparent MIMO antenna

Currently, we notice the mobile phone trend in the market with slim, lightweight, and compact designs. It is expected that futuristic mobile phones may be transparent in their design. To meet this requirement, the antenna in the phone should also be transparent. Quite a few research has been conducted in the field of the transparent antenna and tested the design using fiberglass as a substrate with conducting materials such as indium tin oxide (ITO), and silver-coated polyester film (AgHT) instead of copper. The equations for current flow distribution and analysis parameters for transparent material are presented in Ref. [99]. Here [100,101] are four-port transparent antennas that use indium tin oxide and AgHT-8 as conducting layers. The design in Ref. [100] uses a glass substrate on which two sub-6 GHz antenna and two mmWave antenna are etched. For sub-6 GHz, antenna-1 is a rectangular patch with the full ground, fed by an inset feed of 50 Ω microstrip line. This results in radiation on the broadside with low back radiation in E & H-plane. The antenna-2 has partial ground, fed by a 50 Ω microstrip line, radiates bidirectional in E-plane and omnidirectional in H-plane. For mmWave, antenna-3 is a rectangular patch with the full ground, fed by an inset feed microstrip line resulting in radiation in a broadside direction, whereas antenna-4 is a rectangular patch with the partial ground, fed by a 50 Ω microstrip line, radiates in bidirectional. The design maintains the transparency of 84% with ITO conductive film resistance of 6Ω/sq at 185 nm thickness and electrical conductivity $\rho \sim 9 \times 10^5$ S/m.

In [101], a 4-port MIMO antenna is designed on a plexiglass substrate with a thickness of 1.85 mm, whose transparency is around 85%. AgHT-8 is used as a conductive layer with a conductivity of 125,000 S/m and a thickness of 0.177 mm to maintain the overall transparency. The initial design is a rectangular patch that resonates at 28 GHz and is optimized with an extended rectangular arms stub in the closed path along the side of a rectangular patch, which generates another resonance at 35 GHz. Further, the single-element antenna is extended to a 4-port MIMO positioned adjacent and opposite to each other. The isolation parameter characteristic is studied by varying the distance between the antenna horizontally ($d1 = \lambda_0/2, \lambda_0/3, \lambda_0/4$) and vertically ($d2 = 1$ mm, 2 mm, 3 mm). The performance metrics of these transparent MIMO are as follows: bandwidth 4.7–5 GHz/22.7–28.3 GHz and 23.51–26.54 GHz/33.11–44.02 GHz, gain 3.9 dBi/3.7 dBi and 3 dBi, isolation –32 dB/-35 dB and –16 dB, radiation broadside directional with HPBW of 75° in E- and H-plane [100], and bidirectional with HPBW of 60° in E- and H-plane [101]. The performance metrics of these MIMO antennas and prototype fabrications are shown in Figs. 28–30(a-b).

3.6. Meta-surface/metamaterial-based MIMO antenna

As we have seen in the earlier section, the design has average gain, average isolation, and a low front-to-back ratio. In antenna

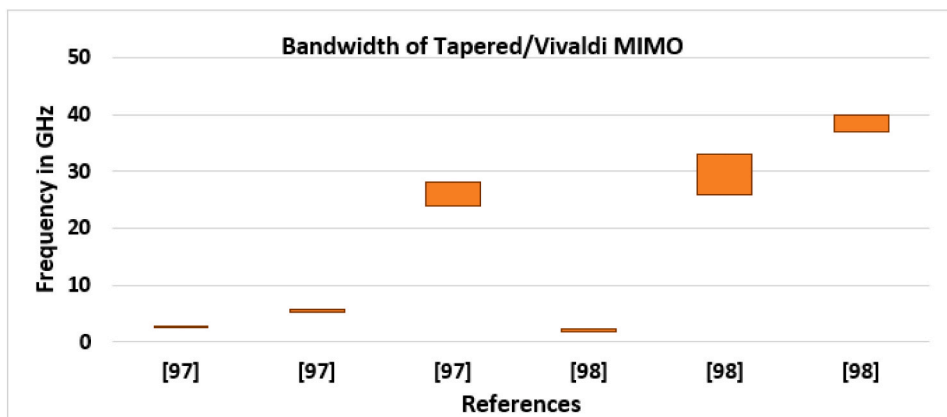


Fig. 24. Performance metrics in terms of bandwidth of tapered/Vivaldi MIMO antennas.

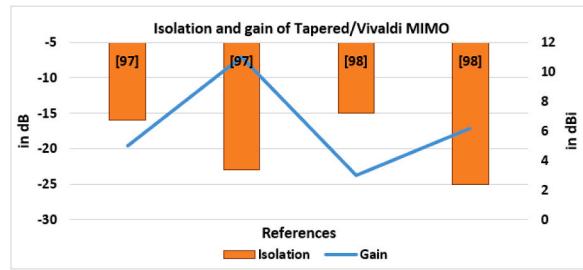


Fig. 25. Performance metrics in terms of isolation and gain of tapered/Vivaldi MIMO antennas.

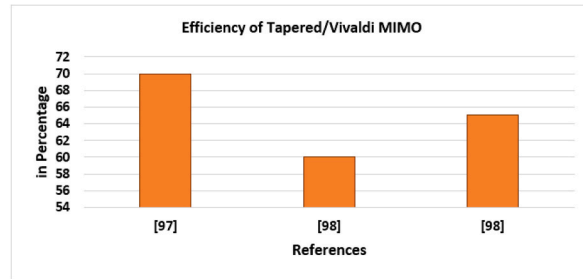


Fig. 26. Performance metrics in terms of efficiency of tapered/Vivaldi MIMO antennas.

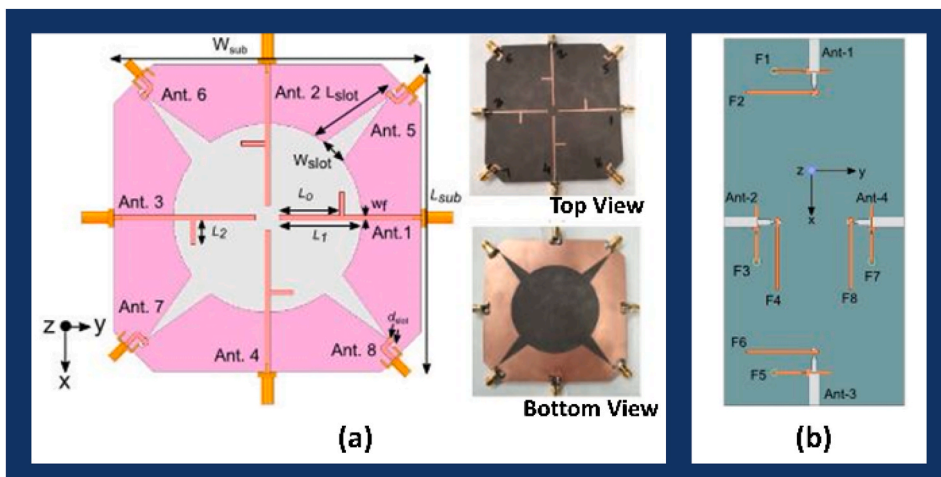


Fig. 27. Design/prototype fabrication of tapered/Vivaldi MIMO antennas, (a) [97], (b) [98].

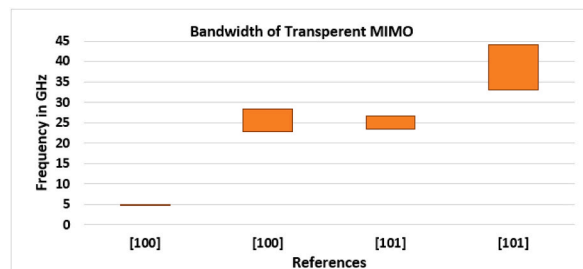


Fig. 28. Performance metrics in terms of bandwidth of transparent MIMO antennas.

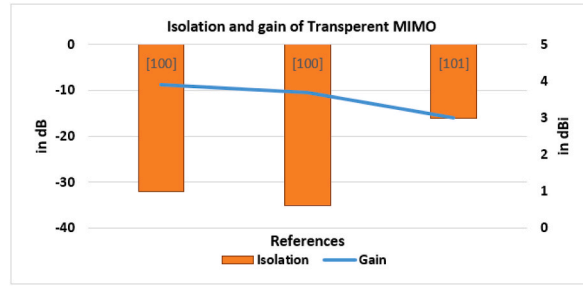


Fig. 29. Performance metrics in terms of isolation and gain of transparent MIMO antennas.

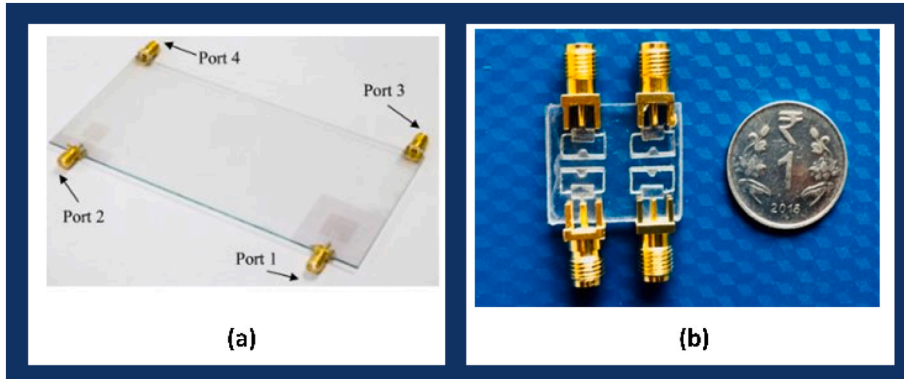


Fig. 30. Prototype fabrication of transparent MIMO antennas, (a) [100], and (b) [101].

design, the better reflection coefficient and isolation are primary requirements that define the bandwidth, gain, and overall performance. In MIMO, these scattering parameters are hampered due to the coupling current from the adjacent antenna and surface waves. Hence, various techniques improve antenna isolation, such as the orthogonal orientation of MIMO elements, parasitic structures, or adapting decoupling structures to reduce the surface wave current [102,103]. The performance of orthogonal-orientated MIMO has been discussed earlier in the DGS section.

This section discusses the performance study of the MIMO antenna loaded with meta-material/meta-surface decoupling structures. The metamaterial structures (such as artificial metamaterial and electromagnetic band gap (EBG)) are etched on the different layers of antenna structure. In contrast, meta-surface are etched on the same plane as of antenna element. Metamaterial is the artificially made material designed [104,105] to change the value of permittivity (ϵ), permeability (μ), and refractive index to a negative value. This can be achieved by a thin wire or split ring structure [106].

The metamaterial structure, such as EBG, when used at the backside of the radiating element, it acts as a reflector to enhance the radiation pattern in the broadside. When the same material is used in the planar structure along with the antenna, then it is referred to as a metasurface (MS) structure. This MS structure can be used along the radiating element to increase the gain and bandwidth by exploiting the surface wave resonance. Also, it provides better isolation between radiating elements.

3.6.1. Meta-surface (MS) structures

Here [107,108], and [109] are MS structures, where radiating element and MS are etched on the same layer. In Ref. [107], a 2×2 MIMO antenna is designed on Rogers 5880 substrate to operate at 28 GHz with circular polarization. The design has a square patch as a radiating element, where one diagonal vertex edge is trimmed to change the polarization from linear to circular. Circular polarization is mostly preferred in satellite communication, WLAN, WIMAX, GPS, and RFIDs [110]. A coaxial feed from the bottom feeds the radiator. The antenna performance is improved by reducing the surface wave losses, for which the periodic structure of MS surrounds the radiating element. The surface wave resonances depend on the number (n) and periodicity (p) of MS unit cells, which can be computed by the transmission line model using equations (1) and (2).

$$\beta_{sw} = \frac{\pi}{L_{cav}} \tag{1}$$

$$L_{cav} = p \times n \tag{2}$$

Where β_{sw} is the propagation constant and L_{cav} is the total length of the MS cavity. The impedance of the MS structure can be computed with the equivalent RLC circuit, where the E-field between the MS unit cells, current flow in MS, and resistivity of MS represents

capacitance, inductance, and resistance effect. After performing the parametric study on the number of MS unit cells, 10×10 MS cells are used with 4-port MIMO.

In [108], a compact 2-port MIMO with a split ring resonator technique is proposed. Here a hexagonal shape radiator is fused with a square split ring resonator (SRR) on top of the Rogers 5880 substrate resulting in an MS unit designed to resonate at 28 GHz. The MS refractive index, permittivity, and permeability are set to zero. At 28 GHz, the surface current in SRR and hexagonal radiator are in opposite directions, which nullifies the current and behaves as a stopband. This design is extended to six-unit MS fed by parallel feed, which is further expanded to 2-port MIMO.

In another approach [109], gain and bandwidth are enhanced through complementary SRR (CSRR) in 4-port MIMO. A single-element rectangular patch is etched on Rogers 6002 substrate with a full ground plane. Performance is optimized by trimming the patch to staircase shape and sides of the ground to partial ground with a rectangular slit at the center. The parametric study on staircase size and ground length is performed for the best results. The single-unit CSRR with negative permeability is designed for the stopband characteristic at 28 GHz. Further, the design is extended to a 4-port MIMO with four CSRR units surrounding each radiating element and one at the ground plane. The performance metrics of these MIMO are as follows: bandwidth 24.5–31 GHz, 24–29.9 GHz, and 25.91–30.22 GHz/35.46–40.45 GHz, gain 11 dBi, 13.4 dBi, and 7 dBi, isolation –31 dB, –24 dB, and –17 dB, and radiation broadside at HPBW of 54° in E– and H-plane [107], 70° in E– and H-plane [108], and omnidirectional [109]. The performance metrics and prototype design are shown in Figs. 31–34(a-c).

3.6.2. Meta-material (MTM) structures

Here [111–114], and [115] presents the MTM structures, which are stacked above or below the radiating layer to improve the antenna performance. The [111] has three substrates of Rogers 4003 with four-layer. The two inverted M-shape patch is etched on top of the upper substrate (S1), a 3×6 metamaterial structure (EBG) is etched on top of the middle substrate (S2), the ground plane is on top of the lower substrate (S3) with feed points and ground at the bottom. These three substrates are joined with the prepreg substrate of Rogers 4450. The metallic vias are used to connect the patch and EBG structure to the bottom of S3. The isolation performance of 3×4 , 3×6 , and 5×6 EBG are studied, where 3×6 has shown better isolation in the band of interest at 25 GHz.

In another design approach, a 4-port, two-layer design supported by MTM to improve the radiation pattern and enhance the gain is proposed [112]. The radiating patch is a combination of two circular rings etched on top of Rogers 5880 substrate. The performance of the reflection coefficient is improved by inserting a slot in the lower ring and a slit in the upper ring. Further, the bandwidth is improved by truncating the full ground plane to partial with a notch in the center. The design is extended to a 4-port MIMO with disconnected grounds. A 2×2 MTM layer is stacked below the radiating elements to improve the performance. The MTM structure has circular patches trimmed on three sides and placed in an orthogonal orientation. The proposed MS unit exhibits negative permittivity and positive permeability with a high refractive index of 20. The flow of surface current in the radiator and MTM are in opposite directions, indicating a good stopband performance at the desired frequency of 26 GHz.

In [113], a 4-port MIMO antenna is backed by an MTM structure (Artificial Magnetic Conductor (AMC)) to improve the gain over the 28 GHz band. The design has a rectangular patch on top of the Rogers RO4003 substrate, fed by a 50Ω microstrip line. The bottom of the substrate has ground that is optimized to partial ground to improve the return loss. Further, resonance enhancement is obtained by trimming along the patch width. The design is extended to 2-port MIMO with orthogonal orientation but with disconnected grounds. An AMC is a square patch with a rectangular slot at the center, which makes it a square SRR, placed on top of the second substrate with the full ground plane at the bottom, designed to resonate at a single frequency. An AMC of 7×7 is stacked below the radiating layer.

A 9×6 circular split ring resonator (SRR) is used as an MTM structure to improve the gain and isolation with the MIMO antenna [114]. Here, single-element is a rectangular patch with inset quarter-wave transformer feed on top of Rogers 5880 substrate. The patch is optimized with a bow-tie slot in a horizontal and vertical direction to improve the impedance matching and shift the resonance to a lower frequency. Further, fine-tuned with a semi-circular slit at the top corners of the patch to obtain the desired band. The design is extended to two element array fed by parallel feed, which is further developed to a 4-port MIMO that shares common ground. To improve the isolation between array elements, a rectangular slot is etched on the ground plane. To further improve the isolation, a layer of SRR-MS is stacked on top of MIMO. The SRR-MS unit cell is made up of two circular split rings with circular geometry designed to resonate at 26 GHz with zero permittivity and permeability. This makes the current flow in the opposite direction in SRR, by which the mutual coupling to the adjacent antenna element is reduced.

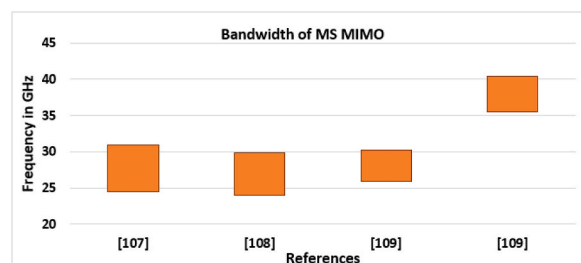


Fig. 31. Performance metrics in terms of bandwidth of MS MIMO antennas.

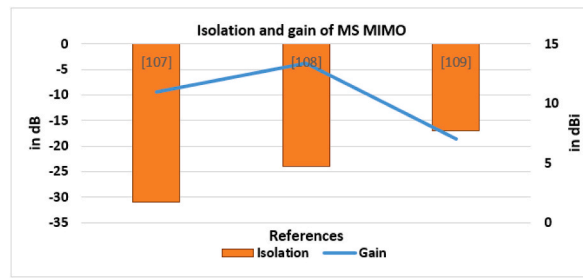


Fig. 32. Performance metrics in terms of isolation and gain of MS MIMO antennas.

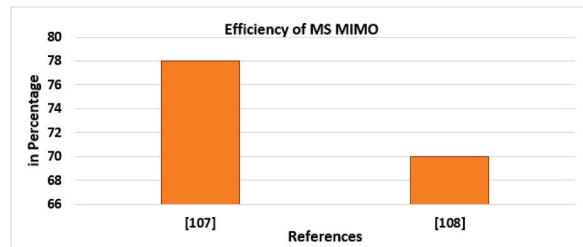


Fig. 33. Performance metrics in terms of efficiency of MS MIMO antennas.



Fig. 34. Prototype fabrication of MS MIMO antennas, (a) [107], (b) [108], and (c) [109].

Similar to the earlier design, a 2-port MIMO, each with three radiating antenna arrays, is backed by an EBG MTM structure to reduce back radiation and to improve the front-to-back (F/B) ratio operating at dual-band 28/38 GHz [115]. The monopole antenna has a rectangular slot in the ground plane and a 50 Ω transmission line with a tuning stub on the other side of the Rogers RO4003C substrate. The stub is added to enhance the impedance match, resulting in a better reflection coefficient S_{ii} of -45 dB and -35 dB at 28 and 38 GHz. A single element is extended to a three-element array and further to 2-port MIMO. Due to the slots in the ground plane, the coupling current is controlled. The slot antenna tends to radiate bidirectionally. This issue is resolved by stacking a layer 15×25 EBG structure placed below the antenna at a distance of $\lambda_0/4$ wavelength. The EBG unit is a circular patch with three slits on four sides. The performance metrics of MTM MIMO antennas are as follows: bandwidth 24.9–29, 23.5–28.5, 26.5–31.5, 24.7–26.7, and 22.5–50 GHz, gain 7 dBi, 10.4 dBi, 9.6 dBi, 9.3 dBi, and 11 dBi, isolation, -23 dB, -26 dB, -25 dB, -36 dB, and -24 dB, radiation broadside at HWPB of 40° and 70° [111], 120° [112], 55° [113], 40° [114] and 90° [115] in E- and H-plane. The performance metrics and

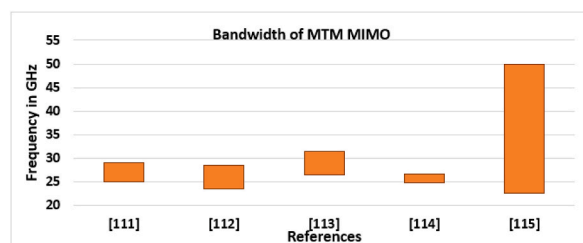


Fig. 35. Performance metrics in terms of bandwidth of MTM MIMO antennas.

prototype fabrication are shown in Figs. 35–38(a-e).

3.6.3. Meta-lens/Fabry-Perot Cavity structures

In all the above designs, the radiation is in the broadside direction, with wide beamwidth. The 5G application requires a narrow beam with beam steering ability to support multiusers at a high data rate. Here [116,117] discusses beamforming structures. In Ref. [116], a meta-lens is used to direct the beam in three directions (-15° , 0° , $+15^\circ$) with an HPBW of 12° from a 2-port MIMO. The antenna structure has two substrates of Rogers 5880, where three-square patches are etched on top of the upper substrate. The patches are fed by a curved microstrip line etched on top of the lower substrate. The patches are optimized with rectangular slot in obtuse angle, resulting in CP. The meta-lens layer is stacked above the antenna structure at a focal length of 12 mm, which decides the beam angle. The meta-lens unit has a cross shape dipole with two circular rings which has four slits. A total of 15×15 meta-lens units are arranged with a gap of 0.05–1.42 mm, to obtain desired transmission magnitude and phase.

Another proposed design attempts the narrow beamwidth and high gain by employing a partially reflecting surface (PRS) above the radiating element by forming a Fabry-Perot Cavity [117]. The Fabry-Perot Cavity antenna has gained attention for mmWave applications because of its directive radiation and compact dimension [118]. Its characterization is studied in Ref. [119]. In Ref. [117], the PRS is positioned half-wavelength above the radiating element, which is determined by the reflection phase at resonance frequency with the thickness of half-wavelength. A single antenna is a square patch on Rogers 5880 substrate whose obtuse angle diagonal corners are trimmed and has a diagonal slot that results in circular polarization (RHCP). The design is extended to 4-port MIMO, where antenna elements are placed in orthogonal orientation for better isolation and fed by coaxial feed to reduce transmission line losses. The partial reflective surface (PSR) is stacked above the antenna layer, separated by an air-filled form. The signal takes multiple reflectional between patch and PSR, which will then be emitted with high directivity. The performance metrics of these MIMO antennas are as follows: bandwidth 28–31.9 GHz and 25.5–33 GHz, gain 18 dBi and 14.1 dBi, isolation -16 dB and -24 dB, and radiation in the broadside with HPBW of 12° and 30° in E- and H-plane with circular polarization. The performance metric and prototype fabrication of these antennas are shown in Figs. 39–41(a-b).

3.7. Dielectric resonator MIMO antenna

Early in the 1980s, the dielectric resonator antenna was demonstrated [120] for the millimeter wave spectrum, which uses the theory of magnetic wall condition. The typical structure uses low dielectric constant material in the form of cylindrical or rectangular shapes placed on the ground plane. The DRA can be fed by probe-fed coaxial feed, microstrip transmission line, or coplanar waveguide (CPW). The details of DRA's shape and various feeding methods are discussed in Ref. [121]. The radiation pattern in DRA will be normal in the direction of the ground plane. The DRA can be designed to have linear polarization, or its geometry can be modified to obtain circular polarization. The DRA with dual-polarized can be obtained by exciting TE mode and TM mode with modified structure [122]. Further, the gain of DRA can be improved by combining meta-material [123]. In this section, DRA MIMO antenna with different isolation techniques in Refs. [124,125], and [126] for mmWave applications are presented.

In [124], two rectangular DRA of Rogers 6010 is placed on the ground plane, where the ground plane is printed on top of the Rogers 5880 substrate. The power to DRA is coupled through a 50Ω microstrip line, etched at the substrate's bottom, coupled through a horizontal rectangular slot in the ground plane underneath DRA. The two DRA are separated by a distance of 1.27 mm from the edges. To improve the isolation, two metallic vias are added vertically at the edges of adjacent DRA, which reduces the coupling current. With two metallic vias, the current coupling to the second DRA is reduced, and the S_{ij} parameter is significantly improved to -50 dB at 26.2 GHz.

In another approach, a metallic strip is pasted on DRA edges to improve the isolation [125]. The design of DRA is the same as in Ref. [124], where the two rectangular DRA of Rogers 5880 are placed on a ground plane which is fed by a printed microstrip line, power coupled through a slotted ground plane. To improve the isolation and reduce the surface wave losses, a microstrip line is etched on DRA. To study the current coupling effect, the 2-port DRA is electrically excited with and without an isolation metallic strip. Due to the metallic strip on DRA, the current concentration drifted from the edges to the metallic strip and the ground plane because of its capacitor-like nature.

In another design [126], a metamaterial structure is used to enhance the isolation in DRA. Here, a 4-port rectangular DRA of Rogers 5880 is placed on the ground plane of the FR4 substrate. A microstrip feed line feeds the DRA through a slotted ground plane. A

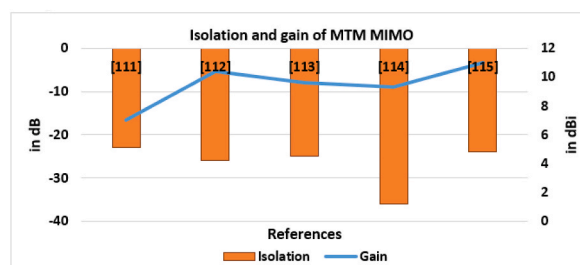


Fig. 36. Performance metrics in terms of isolation and gain of MTM MIMO antennas.

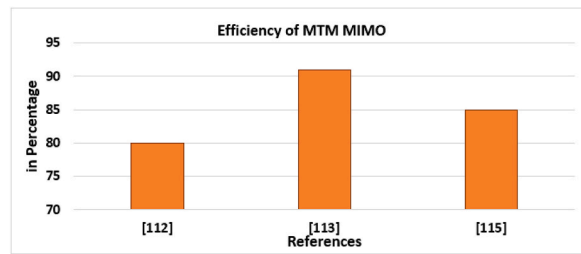


Fig. 37. Performance metrics in terms of efficiency of MTM MIMO antennas.

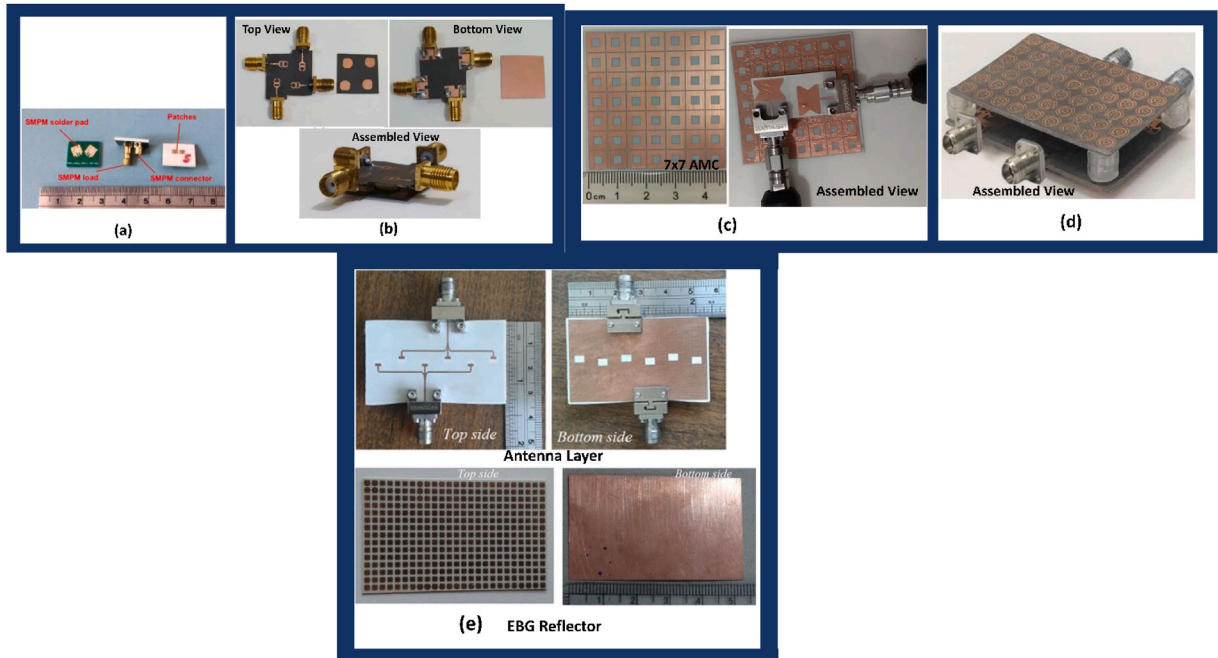


Fig. 38. Prototype fabrication of MTM MIMO antennas, (a) [111], (b) [112], (c) [113], (d) [114], and (e) [115].

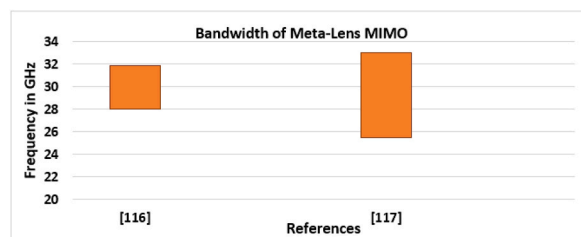


Fig. 39. Performance metrics in terms of bandwidth of meta-lens MIMO antennas.

semi-circular shape metamaterial is engraved on top of the DRA to enhance the isolation S_{12} from -16.07 dB to -29.34 dB and improve the reflection coefficient S_{11} from -35 dB to -46.52 dB at 28 GHz. The performance metrics of DRA MIMO antennas are as follows: bandwidth 25.5–27.2 GHz, 27.5–28.35 GHz, and 26.8–28.8 GHz, gain 6.3 dBi, 8.2 dBi, 5.6 dBi, isolation -32 dB, -24 dB, and -20 dB, radiation at HPBW is 60° [124], omnidirectional [125], and 60° [126] in E- and H-plane. The performance metrics and prototype fabrication are shown in Figs. 42–44(a-c).

3.8. Flexible/wearable MIMO antenna

Wearable electronic gadgets are getting more popular day by day. The antenna should be flexible and designed on flexible

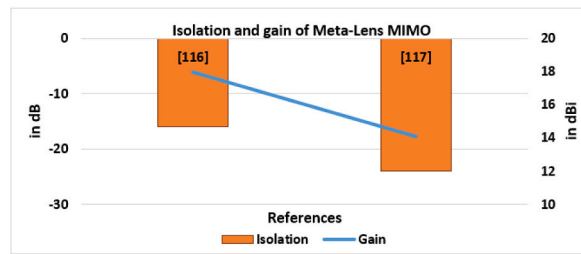


Fig. 40. Performance metrics in terms of isolation and gain of meta-lens MIMO antennas.

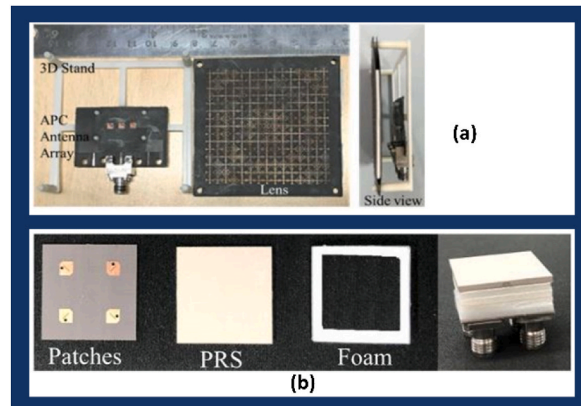


Fig. 41. Prototype fabrication of meta-lens MIMO antennas, (a) [116], and (b) [117].

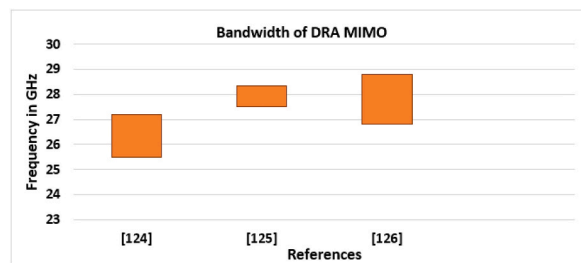


Fig. 42. Performance measure in terms of bandwidth of DRA MIMO antennas.

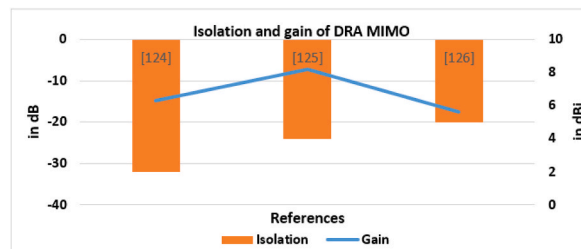


Fig. 43. Performance measure in terms of isolation and gain of DRA MIMO antennas.

substrates or fabrics for such applications. The flexible antennas used in body-worn applications should have a compact design and avoid back radiation which could cause harm to human tissue. In this section [127,128], are flexible antennas, where [127] is a two-element MIMO with a 5×5 MTM structure, and [128] is two element MIMO on a felt substrate.

In [127], the single element is a rectangular patch on top of the Rogers 6002 substrate with the full ground at the bottom. The patch is fed by a 50Ω quarter-wave transformer transmission line. The element is designed to resonate at 24 GHz. The single-element is

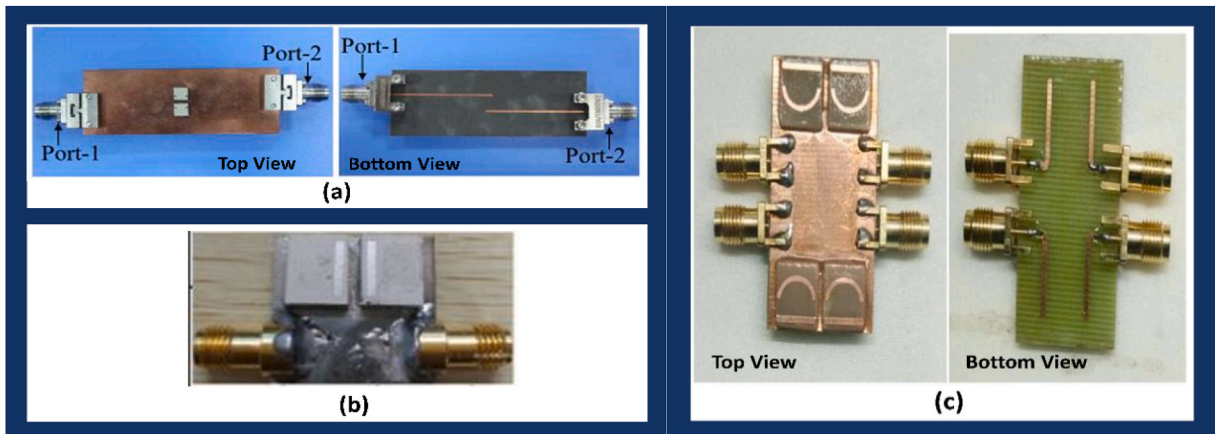


Fig. 44. Prototype fabrication of DRA MIMO antennas, (a) [124], (b) [125], and (c) [126].

extended to two port MIMO, which are placed adjacent at 5.14 mm. The MIMO antenna is backed by EBG (MTM) structure to avoid back radiations. The MTM unit cell is a square patch with a circular slot at the center, corners are semi-circularly trimmed, and edges have rectangular slits. Here, the MTM unit structure is characterized by zero permittivity, permeability, and refractive index. The bending analysis for two-port MIMO with 5×5 MTM has resulted in gain and efficiency variation of 6 dBi to 5.8 dBi, and 80.2%–69.8% over along x and y axis at 60° to 20° and 80° to 60° .

Though SAR is less effective at mmWave, spatial power density analysis is performed in Ref. [127] with and without EBG, which shows peak power densities of 2428.3 W/m^2 and 1800 W/m^2 for 1 W of input power. It indicates that due to EBG, the directivity has been improved, and radiation spread on the skin has also been reduced. In another design, a Felt substrate is used as flexible material of 1 mm thickness. The conductive material for the radiator and ground plane is ShieldiT superconductor, which has a resistivity of $<0.5 \Omega$ per square [128]. Initially, the antenna is designed for a single element of sickle shape with the partial ground, fed by a 50Ω microstrip line. A $\lambda/2$ long stub is added to the right of the ground plane to improve the impedance match and increase the bandwidth. The stub is extended to the left to form an inverted L-shape in the ground plane. Due to this extended stub, it resulted in circular polarization. Finally, a rectangular slit at the center of the ground has resulted in wider bandwidth. The design is extended to two port MIMO, where the two elements are placed in asymmetrical order. This asymmetrical arrangement has formed the T-shape structure in the ground plane. The T-shape structure behaves as decoupling element in MIMO, which is further improved by introducing slit at the center of T-structure. The performance metrics of these flexible MIMO antennas as follows: bandwidth 23.2–24.9 GHz and 3.5–13.5 GHz, gain 5 dBi and 5 dBi, isolation -31 dB and -16 dB , and radiation at HPBW is in broadside at 40° [127] and 90° [128] in E- and H-plane. The performance metrics of these MIMO antennas are shown in Figs. 45–47. The prototype fabrication is shown in Fig. 48(a and b).

3.9. Summary

In the above section, various planar MIMO antenna designs and their performances in terms of bandwidth, gain, isolation, efficiency, and radiation pattern are discussed and presented in the figures. Table 1 summarizes the reviewed MIMO antenna performance along with the structural dimension.

4. Discussions

The focus of this review article is restricted to the discussion of mmWave planar MIMO antenna designs and their performances.

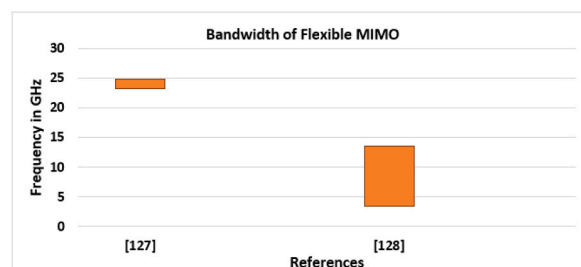


Fig. 45. Performance metrics in terms of bandwidth of flexible MIMO antennas.

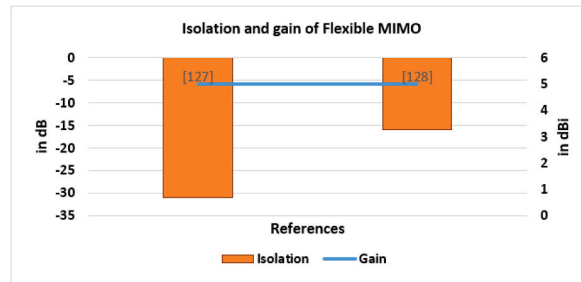


Fig. 46. Performance metrics in terms of bandwidth of flexible MIMO antennas.

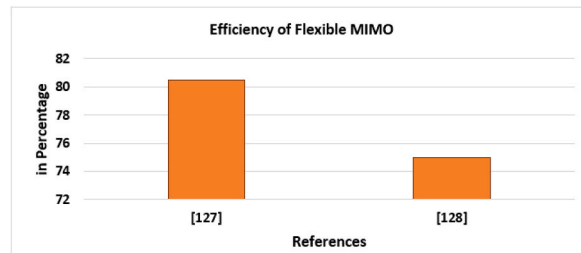


Fig. 47. Performance metrics in terms of efficiency of flexible MIMO antennas.

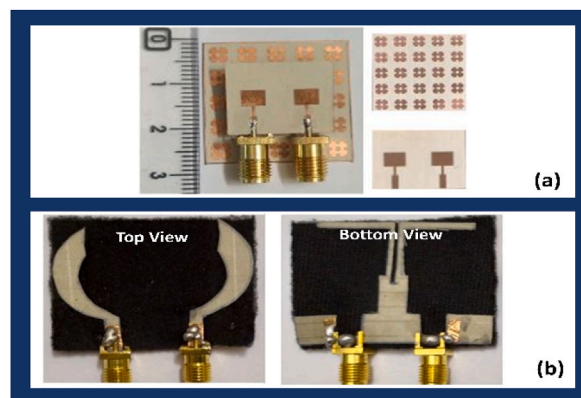


Fig. 48. Prototype fabrication of flexible MIMO antennas, (a) [127] and (b) [128].

The above section already discussed the importance of mmWave in the field of communication, as it offers a broad spectrum and bandwidth, with which a higher data rate can be achieved with low latency. Most of the countries operating at 5G are working with 28 and 38 GHz band, as this band experience lesser attenuation to atmospheric conditions. At mmWave, as the wavelength gets smaller, the antenna size also reduces to a large extent. It is challenging to design such a small antenna because it requires a high degree of precision in etching the conductive layer on the substrate. Any minor modification to the patch or ground will adversely affect the antenna's performance. The single-element antenna at mmWave offers low gain, average bandwidth, and radiation is omnidirectional.

The limitation of a single-element antenna has been overcome by array configuration. The array antennas have increased the gain and radiation performance [37], but the array structure with series-fed and parallel-fed has its limitations in terms of narrow bandwidth, transmission line losses, and substrate losses, and also, the overall design structure is larger.

A properly designed MIMO antenna can overcome the above limitations can result in a compact structure with good performance measures in terms of gain, bandwidth, and radiation. The MIMO antenna with spatial diversity and multiplexing technique can overcome the issue of path loss propagation and support higher data rates.

In this article, six planar slot MIMO antennas are discussed, in which [63,64] have two different types of antenna to resonate at sub-6 GHz and mmWave on the same plane. In Ref. [65], a single antenna can resonate at two different bands but should be excited with two different feeds. The above three designs have larger geometrical structures which is addressed with compact designs in Refs. [66–68]. The gain increases with the number of MIMO ports, as in the case of [57], 20-ports are designed, resulting in a better gain of 12 dBi. The major challenge in MIMO antennas is to control the surface wave current from the adjacent port, which degrades the

Table 1
Summary of MIMO antenna performance parameters.

MIMO Based Antennas											
Reference	Dimension	Center Frequency in GHz	MIMO antenna	MS elements	Gain in dBi	Bandwidth in GHz	Efficiency	Radiation Pattern	Isolation S12 in dB	Beamwidth	Polarization
Slot MIMO Antennas											
[63]	75 × 150 mm ²	1.8/4/28.6	1 × 2/2 × 2/2 × 8	–	4/7/12	1.6–3.2/2.5–2.7/3.3–5/27 - 29	–	Bi-directional/nearly Omni-directional at sub-6 GHz/RHCP at mmWave	–20/- 15/-20	10 ⁰ for RHCP	Circular
[64]	75 × 110 mm ²	5.9/28	1 × 2/2 × 2	–	5.13/9.53	5.29–6.12/26–29.5	83/73	Omni-directional at sub-6 GHz/Broadside at mmWave	–25/-22	80 ⁰ and 50 ⁰ in E– and H-plane	Linear
[65]	60 × 120 mm ²	3/28	1 × 2/1 × 2	–	5/7.6	1.4–1.58/1.82–2.14/2.48–2.9/3.1–3.8/4.4.5/27.7–28.3	86	Bidirectional at sub-6 GHz/Omnidirectional at mmWave	–28	–	Linear
[66]	12.8 × 26 mm ²	28	1 × 2	–	5.8	28–28.6	60	Omnidirectional	–30	–	Linear
[67]	11.4 × 5.3 mm ²	29	1 × 2	–	6	28.8–29.7	85	Broadside directional	–25	40 ⁰ in E– & 30 ⁰ in H-plane	Linear
[68]	80 × 80 mm ²	28/33/38	2 × 2	–	10.5	24–39	70	Broadside direction	–20	60 ⁰ in E– & H-plane at 28 GHz	Linear
Coplanar Waveguide MIMO Antennas											
[70]	14.56 × 9.63 mm ²	28	1 × 2	–	5.8	26.25–30.14	88	End-Fire radiation at –100 ⁰	–30	65 ⁰ in E– & H-plane	Linear
[71]	12 × 25.4 mm ²	28/38	1 × 2	–	6.4/5	26.5–32.7 and 35–38.4	–	Omnidirectional	–13/-24	–	Linear
[72]	56 × 56 mm ²	2.4/5.5/7.5/28	2 × 2	–	6 dB	1.3–40	–	Omnidirectional	–25	–	Linear
[73]	24 × 24 mm ²	31.5	2 × 2	–	5.68	24.8–44.45	85	Omni-directional	–20	–	Linear
Defected Ground Structure MIMO Antennas (non-common ground)											
[78]	26 × 11 mm ²	27/39	1 × 2	–	5/5.7	25–28.2/36.2–41	99.5/98.6	Bidirectional in E-plane and Omnidirectional in H-plane	–30/-25	80 ⁰ in E-plane at 27 GHz	Linear
[79]	26 × 14 × 0.38 mm ³	28/38	1 × 2	–	1.27/1.83	26.65–29.2/36.95–39.05	78/76	Omnidirectional	–20	–	Linear
[80]	30 × 30 mm ²	28	2 × 2	–	6.1	27.6–29.7	92	Omnidirectional	–29	–	Linear
[81]	20 × 24 mm ²	28/38	2 × 2	–	7.9	27.6–28.4/37.9–38.5	85	Broadside direction	–28	35 ⁰ in E– & H-plane at 28 GHz	Linear
[82]	30 × 30 mm ²	28	2 × 2	–	6.5	26–29	85	Omnidirectional	–25	–	Linear
[83]	110 × 55 mm ²	28/38	2 × 2	–	7.95/8.27	27–28/37.2–38.8	89.89/88.25	Broadside direction	–30/-24	60 ⁰ & 90 ⁰ in E-plane at 28 GHz & 38 GHz	Linear
[84]	24 × 24 mm ²	28	2 × 2	–	5.66	23.6–31.5	85	Omnidirectional	–27.5	–	Linear
[85]	20 × 20 mm ³	28	2 × 2	–	8	26.5–30.8	60	Bidirectional	–22.5	110 ⁰ in E-plane	Linear
[86]	24 × 24 mm ²	28/36	2 × 2	–	6.4	24.2–37.8	91	Bidirectional	–27	60 ⁰ & 70 ⁰ in E– & H-plane	Linear
[56]	14 × 14 mm ²	28/38	2 × 2	–	6/5	27–28.8/36–38.7	98	Bidirectional	–30/-32.5	75 ⁰ & 90 ⁰ in E– & H-plane at 28 GHz, 90 ⁰ in E– & H-plane at 38 GHz	Linear
Defected Ground Structure MIMO Antennas (common ground)											
[87]	30 × 15 mm ²	28	1 × 2	–	5	26.5–32.9	84	Bidirectional	–35	–	Linear

(continued on next page)

Table 1 (continued)

MIMO Based Antennas											
Reference	Dimension	Center Frequency in GHz	MIMO antenna	MS elements	Gain in dBi	Bandwidth in GHz	Efficiency	Radiation Pattern	Isolation S12 in dB	Beamwidth	Polarization
[88]	18 × 36 mm ²	–	1 × 2	–	6	3–40	–	Omnidirectional	–20	90° & 60° in E- & H-plane at 28 GHz	Linear
[89]	14 × 20 mm ²	24	1 × 2	–	6.5	17–25	80	Bidirectional	–16	70° in E- & H-plane	Linear
[90]	30 × 52 mm ²	2/6/10/13/15.5	1 × 2	–	3/4.8	1-4/5.5–6.8/9.5–10/12–13.5/14.8–16	–	Bidirectional	–27	–	Linear
[91]	43.61 × 43.61 mm ²	28/38	2 × 4 (4-port)	–	7.9/13.7	27.5–28.9/37.2–38.5	98/92.25	Omi-directional	–25	–	Linear
[55]	30 × 35 mm ²	28	2 × 2 (8 Elements)	–	8.3	25.5–29.6	82	Broadside direction (tilted at –35°)	–17	70° & 55° in E- & H-plane at 27.5 GHz	Linear
[92]	47.5 × 32.5 mm ²	38	2 × 2	–	6.5	37–40	80	Broadside with high side-lobe level	–25	Appx. 120° & 60° in E- & H-plane	Linear
[93]	64.2 × 64.2 mm ²	08	8 - Port	–	5.6	2.84–11	–	Bidirectional at certain frequency and Omnidirectional at certain	–15	–	Linear
[94]	30 × 35 mm ²	28	4-Port	–	11	27.5–28.5	80	Broadside directional (with tilt)	–38	40° & 50° in E- & H-plane	Linear
[95]	24 × 22.5 mm ²	32	4-Port	–	09	27.4–40	42	Omnidirectional	–30	–	Linear
Tapered/Vivaldi MIMO Antennas											
[97]	104 × 104 mm ²	2.45/28	2 × 2/2 × 2	–	5/11	2.45–2.75/5.3–5.7/24–28	70	Broadside directional (90° & 45° tilt at E- & H-plane)	–16/–23	40° in E- & H-plane	Linear
[98]	136 × 68 mm ²	2/28/38	2 × 2/2 × 2	–	3/6.2	1.9–2.3/26–33/37–40	60/65	Omnidirectional sub-6 GHz/Directional at mmWave	–15/–25	60° in E- & H-plane	Linear
Transparent MIMO Antennas											
[100]	150 × 70 mm ²	4.9/26	1 × 2/1 × 2	–	1/3.9/3.7	4.776–5.052/22.7–28.3	–	Broadside directional	–32/–35	75° & 60° in E- & H-plane	Linear
[101]	24 × 20 mm ²	28/38	2 × 2	–	3	23.51–26.54/33.11–44.02	75	Bidirectional	–16	60° in E & H-plane	Linear
Meta-surface/Metamaterial MIMO Antennas											
[107]	27.5 × 27.5 mm ²	27.5	2 × 2	10 × 10	11	24.5–31	78	Broadside with low side lobes (Tilted by 30°)	–31	54° in E- & H-plane	Circular
[108]	52 × 23 mm ²	28	1 × 2	3 × 6	13.40	24–29.9	70	Broad side with tilt at ± 30 Deg	–24	70° in E- & H-Plane	Linear
[109]	30 × 30 mm ²	28/38	2 × 2	4 × 4	7	25.91–30.22/35.46–40.45	–	Omnidirectional	–17	–	Linear
[111]	15 × 12.7 mm ²	27	1 × 2	3 × 6	7	24.9–29	–	Broadside directional	–23	40° & 70° in E- & H-plane	Linear
[112]	12 × 10 mm ² /22 × 24 mm ²	26	2 × 2	2 × 2	10.4	23.5–28.5	80	Broadside with low minor lobe	–26	120° in E- & H-plane	Linear
[113]	47 × 47 mm ²	28	2 × 2	7 × 7	9.6	26.5–31.5	91	Broadside with two Major lobes at ± 30 Deg	–25	55° in E- & H-Plane	Linear
[114]	30 × 43 mm ²	26	2 × 2	9 × 6	9.3	24.7–26.7	–	Broadside directional	–36	40° in E- & H-plane	Linear
[115]		28/38		15 × 25		22.5–50	85	Broadside directional	–24	90° in E- & H-Plane	Linear

(continued on next page)

Table 1 (continued)

MIMO Based Antennas											
Reference	Dimension	Center Frequency in GHz	MIMO antenna	MS elements	Gain in dBi	Bandwidth in GHz	Efficiency	Radiation Pattern	Isolation S12 in dB	Beamwidth	Polarization
	53 × 31.7 mm ²		2-port with 4 array elements		11.5/10.9 at 28/38 GHz						
[116]	60 × 60 mm ²	28	1 × 3	15 × 15	18	28–31.9	–	Broadside directional	–16	12 ⁰ in E– & H-plane	Circular RHCP
[117]	16.92 × 16.92 mm ²	28	2 × 2	1 × 1	14.1	25.5–33	–	Broadside directional	–24	30 ⁰ in E– & H-plane	Circular
DRA MIMO Antennas											
[124]	21.77 × 11 mm ²	26	1 × 2	2 × 2	6.3	25.5–27.2	–	Broadside directional	–32	60 ⁰ in E– & H-Plane	Linear
[125]	20 × 20 mm ²	28	1 × 2	1 × 2	8.2	27.5–28.35	–	omnidirectional	–24	–	Linear
[126]	20 × 40 mm ²	28	2 × 2	2 × 2	5.6	26.8–28.8	88	Bi-directional	–20	60 ⁰ E– & H-plane	Linear
Flexible MIMO Antennas											
[127]	19.04 × 15.06 mm ²	24	1 × 2	5 × 5	5	23.2–24.9	80.5	Broadside directional (Tilted by 30 ⁰)	–31	40 ⁰ in E– & H-plane	Linear
[128]	42 × 32.5 mm ²	06	1 × 2	–	5	3.5–13.5	75	Directional in Broadside with tilt at ± 30 deg in E & H plane	–16	90 ⁰ in E– & H-plane	Circular

overall antenna performance. It is evident from Fig. 12 that the asymmetrical arrangement of elements of unique shape in Ref. [66] has increased the isolation to -30 dB but with reduced gain. The other method to increase the isolation is through the orthogonal orientation of elements, as in Ref. [68].

The designs in Refs. [70–72], and [73] are CPW structures where the transmission line/radiating element and ground are in the same plane. The CPW technique reduces the substrate losses, transmission line losses, or ohmic losses which result from the series-fed or parallel-feed method. In Refs. [70,71], the ground points between ports are not common, which is evident that coupling will be low and isolation will be high. In this case, it has -35 dB and -25 dB of S_{ij} , such designs are not preferred in 5G applications. Though [72, 73] share the common ground, isolation level S_{ij} is higher at -25 dB and -20 due to its unique design structure. It also has resulted in wide bandwidth as in Fig. 15.

The other method to improve the performance of the MIMO antenna in terms of bandwidth and isolation is through defected ground structure, where the ground plane is optimized to obtain the desired results. In Refs. [78–86], and [56] are DGS structures that don't share common ground, whereas [55,87–94], and [95] has the common ground point. All these designs have shown a good bandwidth of 1 GHz and above with good isolation S_{ij} level of -15 dB to -35 dB.

In [97], the single tapered structure is designed to resonate at two largely separated bands which are fed by two separate feeds, whereas in Ref. [98], the tapered structure acts as isolating structure at the lower band (sub-6 GHz) and as a resonator at mmWave. Both these structures have resulted in good bandwidth and isolation at mmWave as in Figs. 26 and 27.

As the transparent handsets might be futuristic, in Refs. [100,101], transparent MIMO antennas are designed, which used indium-tin-oxide and AgHT-8 as conductive layers instead of copper, and chose glass substrate for transparency. Both designs have resulted in good bandwidth and isolation but with low gain, as shown in Figs. 28 and 29. The transparent conducting material is expensive at present, which is why limited research work can be seen on these structures for mmWave.

As discussed before, orthogonal orientation is one of the methods to reduce the coupling effect in MIMO. The other method is to adopt for decoupling structure such as meta-surface/metamaterials. The MS units share the plane with radiating elements as in Refs. [107,108], whereas, in Refs. [111–114], and [115,116], and [117] the MTM structures and meta-lens are stacked above or below the radiating structure. These designs have improved the isolation, gain, bandwidth, and radiation in broadside directions with a narrow beam. The reader can find more details on decoupling structures and the characterization of metamaterial structures in Refs. [102,103, 105,106,129].

Due to reduced dielectric losses, the DRA antennas are very well used in mobile, satellite, and radar applications. The performance of DRA in Refs. [124,125], and [126] is considerably better. The metallic vias and microstrip lines in DRA are implemented to improve the isolation level in these designs. The body-worn flexible antennas are gaining popularity, because of which flexible substrates like Rogers 6002 and felt substrates are used in Refs. [127,128].

However, as discussed in section II, the MIMO antenna design must be evaluated based on six diversity parameters, where most of the designs perform only a few diversity measures. Also, the performance of most designs presented in this article has found wide beamwidth, average gain, varying isolation throughout the band of interest, and few designs lack a common ground point. These key observations are summarized in Fig. 49.

5. Conclusion and future scope

The focus of this article is to provide insight into various designs of the planar MIMO antennas for mmWave applications. The analysis of the existing MIMO antennas highlights the challenges to be overcome. The article has discussed the optimization techniques and effects, decoupling structures (metamaterial) which enhance the performance of MIMO antenna. The mmWave and MIMO technology will be a futuristic communication system to support colossal data demand.

Hence, the 5G application requires the MIMO antennas to operate at wide bandwidth, with high gain and narrow directional radiation. Therefore, future MIMO designs should focus on resolving the issues mentioned in the key observation Fig. 49. For this, the



Fig. 49. Key observation points obtained from the comprehensive review.

compact MIMO antenna design is essential to meet the diversity parameters. The other key point for MIMO antennas is to maintain the constant voltage across all the ports through the common ground for efficient performance.

Also, the designs discussed in this article have used Rogers/FR – 4 as the dielectric substrate (except [100,101]). The geopolymers are other alternatives that can be used as a dielectric substrate to obtain wide bandwidth [130]. Wearable devices are getting popular these days that demand flexible substrates such as Rogers 6006 or fabrics. These antennas have a major challenge in performance consistency against bending losses and variations in radiation. Limited work has been contributed to the field of flexible MIMO antenna at mmWave, and interested researchers can look forward to developing new designs.

The antennas with beam steering capability are the demand for 5G applications which can be performed with the RF p-i-n diodes [131] or phase shift method, or beam switchable method [132]. Beam steering techniques are currently developed for base stations with large antenna profiles. Hence there is a need for optimization such that this technique can be implemented in handheld devices.

Also, graphene can be used instead of copper as a conductive layer because it has good electromagnetic properties [133]. Hence, there is a scope for optimization of the design to fulfill these limitations of earlier methods.

Author contribution statement

All authors listed have significantly contributed to the development and the writing of this article.

Funding statement

This research did not receive any specific grant from funding agencies in the public, commercial, or not-for-profit sectors.

Data availability statement

No data was used for the research described in the article.

Declaration of interest's statement

The authors declare no competing interests.

References

- [1] 5g spectrum sold, get ready to roll out for consumers: centre to telcos, NDTV.com, <https://www.ndtv.com/business/5g-update-5g-spectrum-sold-get-ready-to-roll-out-for-consumers-centre-to-telcos-3264323>. accessed Sep. 01, 2022.
- [2] 5G Spectrum Auction Ends, Govt Earns Over Rs 1.5 Lakh Cr; Reliance Jio Top Bidder, The Indian Express, Aug. 01, 2022. <https://indianexpress.com/article/business/india-concludes-19-bln-5g-spectrum-auction-8064216/>. accessed Sep. 01, 2022).
- [3] I.T.U. Statistics. <https://www.itu.int:443/en/ITU-D/Statistics/Pages/stat/default.aspx>. (Accessed 27 April 2022) accessed.
- [4] World internet users statistics and 2022 world population stats. <https://www.internetworldstats.com/stats.htm> accessed Jun. 13, 2022).
- [5] D. Brenner, "Global 5G Spectrum Update," *SVP, Spectrum Strategy & Technology Policy*, p. 28.
- [6] S. Forge, K. Vu, Forming a 5G strategy for developing countries: a note for policy makers, Aug, Telecommun. Pol. 44 (7) (2020) 101975, <https://doi.org/10.1016/j.telpol.2020.101975>.
- [7] Z. Pi, F. Khan, An introduction to millimeter-wave mobile broadband systems, *IEEE Commun. Mag.* 49 (6) (Jun. 2011) 101–107, <https://doi.org/10.1109/MCOM.2011.5783993>.
- [8] Most internet users by country," Statista. <https://www.statista.com/statistics/262966/number-of-internet-users-in-selected-countries/> accessed Jun. 13, 2022).
- [9] J. Du, R.A. Valenzuela, How much spectrum is too much in millimeter wave wireless access, *IEEE J. Sel. Area. Commun.* 35 (7) (2017) 1444–1458, Jul, <https://doi.org/10.1109/JSAC.2017.2698859>.
- [10] D. Wu, J. Wang, Y. Cai, M. Guizani, Millimeter-wave multimedia communications: challenges, methodology, and applications, *IEEE Commun. Mag.* 53 (1) (Jan. 2015) 232–238, <https://doi.org/10.1109/MCOM.2015.7010539>.
- [11] R. Ford, M. Zhang, M. Mezzavilla, S. Dutta, S. Rangan, M. Zorzi, Achieving ultra-low latency in 5G millimeter wave cellular networks, *IEEE Commun. Mag.* 55 (3) (Mar. 2017) 196–203, <https://doi.org/10.1109/MCOM.2017.1600407CM>.
- [12] X. Liu, Z. Cai, Advanced Obstacles Detection and Tracking by Fusing Millimeter Wave Radar and Image Sensor Data, Gyeonggi-do, Oct. 2010, pp. 1115–1120, <https://doi.org/10.1109/ICCAS.2010.5669740>. *ICCAS 2010*.
- [13] M.T. Bevacqua, S. Di Meo, L. Crocco, T. Isernia, M. Pasian, Millimeter-waves breast cancer imaging via inverse scattering techniques, *IEEE J. Electromagn. RF Microw. Med. Biol.* 5 (3) (Sep. 2021) 246–253, <https://doi.org/10.1109/JERM.2021.3052096>.
- [14] J.E. Johnson, O. Shay, C. Kim, C. Liao, Wearable millimeter-wave device for contactless measurement of arterial pulses, *IEEE Trans. Biomed. Circuits Syst.* 13 (6) (2019) 1525–1534, Dec, <https://doi.org/10.1109/TBCAS.2019.2948581>.
- [15] J.F. Harvey, M.B. Steer, T.S. Rappaport, Exploiting high millimeter wave bands for military communications, applications, and design, *IEEE Access* 7 (2019) 52350–52359, <https://doi.org/10.1109/ACCESS.2019.2911675>.
- [16] Z. Xiao, et al., A survey on millimeter-wave beamforming enabled UAV communications and networking, *IEEE Commun. Surv. Tutorials* 24 (1) (2022) 557–610, <https://doi.org/10.1109/COMST.2021.3124512>.
- [17] M.H. Mazaheri, S. Ameli, A. Abedi, O. Abari, A millimeter wave network for billions of things, Beijing China, in: Proceedings of the ACM Special Interest Group on Data Communication, Aug. 2019, pp. 174–186, <https://doi.org/10.1145/3341302.3342068>.
- [18] Z. Qingling, J. Li, Rain attenuation in millimeter wave ranges, in: *International Symposium on Antennas, Propagation & EM Theory*, 2006, p. 4.
- [19] A.I. Sulyman, A.T. Nassar, M.K. Samimi, G.R. Maccartney, T.S. Rappaport, A. Alsanie, Radio propagation path loss models for 5G cellular networks in the 28 GHz and 38 GHz millimeter-wave bands, *IEEE Commun. Mag.* 52 (9) (Sep. 2014) 78–86, <https://doi.org/10.1109/MCOM.2014.6894456>.
- [20] M.K. Samimi, T.S. Rappaport, G.R. MacCartney, Probabilistic omnidirectional path loss models for millimeter-wave outdoor communications, *IEEE Wireless Commun. Lett.* 4 (4) (Aug. 2015) 357–360, <https://doi.org/10.1109/LWC.2015.2417559>.
- [21] M.C. Kestwal, S. Joshi, L.S. Garia, Prediction of rain attenuation and impact of rain in wave propagation at microwave frequency for tropical region (uttarakhand, India), *Jun. Int. J. Microw. Sci. Techn.* 2014 (2014) 1–6, <https://doi.org/10.1155/2014/958498>.

- [22] M. Marcus, B. Pattan, Millimeter wave propagation: spectrum management implications, Jun, *IEEE Microwave* 6 (2) (2005) 54–62, <https://doi.org/10.1109/MMW.2005.1491267>.
- [23] P. Zhang, J. Li, H. Wang, W. Hong, Measurement-based propagation characteristics at 28 GHz and 39 GHz in suburban environment, Jul, in: 2019 IEEE International Symposium on Antennas and Propagation and, USNC-URSI Radio Science Meeting, Atlanta, GA, USA, 2019, pp. 2121–2122, <https://doi.org/10.1109/APUSNCURSINRSM.2019.8889362>.
- [24] M. Khalily, M. Ghoraiishi, S. Taheri, S. Payami, R. Tafazolli, Millimeter-wave directional path loss models in the 26 GHz, 32 GHz, and 39 GHz bands for small cell 5G cellular system, 17, in: 12th European Conference on Antennas and Propagation, EuCAP 2018), London, UK, 2018, p. 17, <https://doi.org/10.1049/cp.2018.0376>.
- [25] A.M. Al-Samman, et al., Millimeter wave propagation measurements and characteristics for 5G system, Jan, *Appl. Sci.* 10 (1) (2020) 335, <https://doi.org/10.3390/app10010335>.
- [26] R. Dybdal, Millimeter wave antenna technology, *IEEE J. Sel. Area. Commun.* 1 (4) (Sep. 1983) 633–644, <https://doi.org/10.1109/JSAC.1983.1145968>.
- [27] S.M. Shamim, U.S. Dina, N. Arafin, S. Sultana, Design of efficient 37 GHz millimeter wave microstrip patch antenna for 5G mobile application, *Plasmonics* 16 (4) (2021) 1417–1425, Aug, <https://doi.org/10.1007/s11468-021-01412-x>.
- [28] Y. Ghazaoui, A.E. Alami, M.E. Ghzaoui, S. Das, D. Barad, S. Mohapatra, Millimeter wave antenna with enhanced bandwidth for 5G wireless application, *T01003, J. Inst. Met.* 15 (1) (Jan. 2020) T01003, <https://doi.org/10.1088/1748-0221/15/01/T01003>.
- [29] N. Hussain, M. Jeong, J. Park, S. Rhee, P. Kim, N. Kim, A compact size 2.9–23.5 GHz microstrip patch antenna with WLAN band-rejection, *Microw. Opt. Technol. Lett.* 61 (5) (May 2019) 1307–1313, <https://doi.org/10.1002/mop.31708>.
- [30] M.J. Jeong, N. Hussain, J.W. Park, S.G. Park, S.Y. Rhee, N. Kim, Millimeter-wave microstrip patch antenna using vertically coupled split ring metaplate for gain enhancement, *Microw. Opt. Technol. Lett.* 61 (10) (2019) 2360–2365, Oct, <https://doi.org/10.1002/mop.31908>.
- [31] A. Desai, T. Upadhyaya, R. Patel, Compact wideband transparent antenna for 5G communication systems, *Microw. Opt. Technol. Lett.* 61 (3) (Mar. 2019) 781–786, <https://doi.org/10.1002/mop.31601>.
- [32] N. Hussain, M.-J. Jeong, A. Abbas, T.-J. Kim, N. Kim, A metasurface-based low-profile wideband circularly polarized patch antenna for 5G millimeter-wave systems, *IEEE Access* 8 (2020) 22127–22135, <https://doi.org/10.1109/ACCESS.2020.2969964>.
- [33] K. Sultan, M. Ikram, N. Nguyen-Trong, A multiband multibeam antenna for sub-6 GHz and mm-wave 5G applications, *Antennas Wirel. Propag. Lett.* 21 (6) (2022) 1278–1282, Jun, <https://doi.org/10.1109/LAWP.2022.3164627>.
- [34] M. Ikram, N. Nguyen-Trong, A.M. Abbosh, Realization of a tapered slot array as both decoupling and radiating structure for 4G/5G wireless devices, *IEEE Access* 7 (2019) 159112–159118, <https://doi.org/10.1109/ACCESS.2019.2950660>.
- [35] H. Jiang, L.-M. Si, W. Hu, X. Lv, A symmetrical dual-beam bowtie antenna with gain enhancement using metamaterial for 5G MIMO applications, *Feb, IEEE Photonics J* 11 (1) (2019) 1–9, <https://doi.org/10.1109/JPHOT.2019.2891003>.
- [36] R.L. Haupt, Y. Rahmat-Samii, Antenna array developments: a perspective on the past, present and future, *Feb, IEEE Antenn. Propag. Mag.* 57 (1) (2015) 86–96, <https://doi.org/10.1109/MAP.2015.2397154>.
- [37] E. Levine, G. Malamud, S. Shtrikman, D. Treves, A study of microstrip array antennas with the feed network, *Apr, IEEE Trans. Antenn. Propag.* 37 (4) (1989) 426–434, <https://doi.org/10.1109/8.24162>.
- [38] R.J. Mailloux, Antenna array architecture, *Jan, Proc. IEEE* 80 (1) (1992) 163–172, <https://doi.org/10.1109/5.119575>.
- [39] P. Hannan, The element-gain paradox for a phased-array antenna, *Jul, IEEE Trans. Antenn. Propag.* 12 (4) (1964) 423–433, <https://doi.org/10.1109/TAP.1964.1138237>.
- [40] J.G. Andrews, et al., What will 5G Be? *IEEE J. Sel. Area. Commun.* 32 (6) (2014) 1065–1082, Jun, <https://doi.org/10.1109/JSAC.2014.2328098>.
- [41] H. Wang, K.E. Kedze, I. Park, A high-gain and wideband series-fed angled printed dipole array antenna, *IEEE Trans. Antenn. Propag.* 68 (7) (2020) 5708–5713, Jul, <https://doi.org/10.1109/TAP.2020.2975882>.
- [42] U. Ullah, M. Al-Hasan, S. Koziel, I.B. Mabrouk, A series inclined slot-fed circularly polarized antenna for 5G 28 GHz applications, *Antennas Wirel. Propag. Lett.* 20 (3) (Mar. 2021) 351–355, <https://doi.org/10.1109/LAWP.2021.3049901>.
- [43] M.E. Munir, et al., A new mm-wave antenna array with wideband characteristics for next generation communication systems, *May, Electronics* 11 (10) (2022) 1560, <https://doi.org/10.3390/electronics11101560>.
- [44] I. Ahmad, H. Sun, U. Rafique, Z. Yi, Triangular slot-loaded wideband planar rectangular antenna array for millimeter-wave 5G applications, *Mar, Electronics* 10 (7) (2021) 778, <https://doi.org/10.3390/electronics10070778>.
- [45] M. Patriotis, F.N. Ayoub, Y. Tawk, J. Costantine, C.G. Christodoulou, A millimeter-wave frequency reconfigurable circularly polarized antenna array, *IEEE Open J. Antennas Propag.* 2 (2021) 759–766, <https://doi.org/10.1109/OJAP.2021.3090908>.
- [46] S. Trinh-Van, J.M. Lee, Y. Yang, K.-Y. Lee, K.C. Hwang, A sidelobe-reduced, four-beam array antenna fed by a modified 4x4 butler matrix for 5G applications, *IEEE Trans. Antenn. Propag.* 67 (7) (2019) 4528–4536, Jul, <https://doi.org/10.1109/TAP.2019.2905783>.
- [47] Q. Lv, Y.-H. Yang, S.-G. Zhou, C. Shao, D. Zhou, C.-Y.-D. Sim, Design of a single-layer $\pm 45^\circ$ dual-polarized directional array antenna for millimeter wave applications, *Jun, Sensors* 21 (13) (2021) 4326, <https://doi.org/10.3390/s21134326>.
- [48] T.S. Rappaport, *Wireless Communications: Principles and Practice*, vol. 2, prentice hall PTR, New Jersey, 1996.
- [49] Antenna diversity for mobile terminals - ProQuest." <https://www.proquest.com/openview/3f969231fa587781338110e26855672d/1?cbi=51922&diss=y&pq-origsite=gscholar&parentSessionId=Aj7NuDocOvEUu4F%2BaN9suJZFUQgNpNGR%2FHkdsL%2FOJ4%3D> (accessed May 07, 2022).
- [50] J.D. Parsons, M. Henze, M.J. Withers, Diversity techniques for mobile RadiRo eception, *IEEE Trans. Veh. Technol.* 25 (1976) 75–85.
- [51] Lizhong Zheng, D.N.C. Tse, Diversity and multiplexing: a fundamental tradeoff in multiple-antenna channels, *IEEE Trans. Inf. Theor.* 49 (5) (May 2003) 1073–1096, <https://doi.org/10.1109/TIT.2003.810646>.
- [52] G. Casu, L. Tuta, I. Nicolaescu, C. Moraru, Some aspects about the advantages of using MIMO systems, *Nov, in: 2014 22nd Telecommunications Forum Telfor (TELFOR)*, Belgrade, Serbia, 2014, pp. 320–323, <https://doi.org/10.1109/TELFOR.2014.7034415>.
- [53] Y. Long, Z. Chen, J. Fang, Nonasymptotic analysis of capacity in massive MIMO systems, *IEEE Wett.ire. Commun. LETTERS* 4 (5) (2015) 4.
- [54] W. Lee, Mutual coupling effect on maximum-ratio diversity combiners and application to mobile radio, *IEEE Trans. Commun.* 18 (6) (Dec. 1970) 779–791, <https://doi.org/10.1109/TCOM.1970.1090428>.
- [55] M. Khalid, et al., 4-Port MIMO antenna with defected ground structure for 5G millimeter wave applications, *Electronics* 9 (1) (Jan. 2020) 71, <https://doi.org/10.3390/electronics9010071>.
- [56] A. Khabba, J. Amadid, S. Ibynaich, A. Zeroual, Pretty-small four-port dual-wideband 28/38 GHz MIMO antenna with robust isolation and high diversity performance for millimeter-wave 5G wireless systems, *Jul, Analog Integr. Circuits Signal Process.* 112 (1) (2022) 83–102, <https://doi.org/10.1007/s10470-022-02045-8>.
- [57] Q. Rubani, S.H. Gupta, A. Rajawat, A compact MIMO antenna for WBAN operating at Terahertz frequency, *Optik* 207 (Apr. 2020) 164447, <https://doi.org/10.1016/j.ijleo.2020.164447>.
- [58] P. Kumar, T. Ali, M.P. MM, Highly isolated ultrawideband multiple input and multiple output antenna for wireless applications, *Eng. Sci.* (2021), <https://doi.org/10.30919/es8d570>.
- [59] Release 17." <https://www.3gpp.org/release-17> (accessed Sep. 02, 2022).
- [60] A. Dastranj, H. Abiri, Bandwidth enhancement of printed E-shaped slot antennas fed by CPW and microstrip line, *IEEE Trans. Antenn. Propag.* 58 (4) (2010) 1402–1407, Apr, <https://doi.org/10.1109/TAP.2010.2041164>.
- [61] K.-F. Tong, T.-P. Wong, Circularly polarized U-slot antenna, *IEEE Trans. Antenn. Propag.* 55 (8) (2007) 2382–2385, <https://doi.org/10.1109/TAP.2007.901930>.
- [62] Wen-Ling Chen, Guang-ming wang, and chen-xin zhang, "bandwidth enhancement of a microstrip-line-fed printed wide-slot antenna with a fractal-shaped slot, *IEEE Trans. Antenn. Propag.* 57 (7) (2009) 2176–2179, <https://doi.org/10.1109/TAP.2009.2021974>.

- [63] S.P. Biswal, S.K. Sharma, S. Das, Collocated microstrip slot MIMO antennas for cellular bands along with 5G phased array antenna for user equipments (UEs), *IEEE Access* 8 (2020) 209138–209152, <https://doi.org/10.1109/ACCESS.2020.3038328>.
- [64] S. Iffat Naqvi, et al., Integrated LTE and millimeter-wave 5G MIMO antenna system for 4G/5G wireless terminals, *Sensors* 20 (14) (2020) 3926, <https://doi.org/10.3390/s20143926>.
- [65] R. Hussain, et al., A multiband shared aperture MIMO antenna for millimeter-wave and sub-6GHz 5G applications, *Sensors* 22 (5) (1808, Feb) 2022, <https://doi.org/10.3390/s22051808>.
- [66] D. El Hadri, A. Zakriti, A. Zugari, M. El Ouahabi, J. El Aoufi, High isolation and ideal correlation using spatial diversity in a compact MIMO antenna for Fifth-generation applications, *Jul, Int. J. Antenn. Propag.* 2020 (2020) 1–10, <https://doi.org/10.1155/2020/2740920>.
- [67] A. Ahmad, D. Choi, S. Ullah, A compact two elements MIMO antenna for 5G communication, *Sci. Rep.* 12 (1) (Dec. 2022) 3608, <https://doi.org/10.1038/s41598-022-07579-5>.
- [68] D.A. Sehrai, et al., A novel high gain wideband MIMO antenna for 5G millimeter wave applications, *Electronics* 9 (6) (Jun. 2020) 1031, <https://doi.org/10.3390/electronics9061031>.
- [69] R.N. Simons, S. Technology, B. Park, R.Q. Lee, Coplanar waveguide feeds for phased array antennas, in: *Conference on Advanced SEI Technologies, Sep. 1991*, p. 3422.
- [70] H. Zahra, W.A. Awan, W.A.E. Ali, N. Hussain, S.M. Abbas, S. Mukhopadhyay, A 28 GHz broadband helical inspired end-fire antenna and its MIMO configuration for 5G pattern diversity applications, *Electronics* 10 (4) (Feb. 2021) 405, <https://doi.org/10.3390/electronics10040405>.
- [71] M. Venkateswara Rao, B.T.P. Madhav, J. Krishna, Y. Usha Devi, T. Anilkumar, B. Prudhvi Nadh, CSRR-loaded T-shaped MIMO antenna for 5G cellular networks and vehicular communications, *Aug, Int. J. RF Microw. Computer-Aided Eng.* 29 (8) (2019), <https://doi.org/10.1002/mmce.21799>.
- [72] P. Kumar, S. Urooj, A. Malibari, Design and implementation of quad-element super-wideband MIMO antenna for IoT applications, *IEEE Access* 8 (2020) 226697–226704, <https://doi.org/10.1109/ACCESS.2020.3045534>.
- [73] A. Patel, et al., UWB CPW fed 4-port connected ground MIMO antenna for sub-millimeter-wave 5G applications, *Alex. Eng. J.* 61 (9) (2022) 6645–6658, Sep, <https://doi.org/10.1016/j.aej.2021.12.015>.
- [74] W.N. Hardy, L.A. Whitehead, Split-ring resonator for use in magnetic resonance from 200–2000 MHz, *Rev. Sci. Instrum.* 52 (2) (Feb. 1981) 213–216, <https://doi.org/10.1063/1.1136574>.
- [75] R. Marques, F. Mesa, J. Martel, F. Medina, Comparative analysis of edge- and broadside-coupled split ring resonators for metamaterial design - theory and experiments, *IEEE Trans. Antenn. Propag.* 51 (10) (2003) 2572–2581, Oct, <https://doi.org/10.1109/TAP.2003.817562>.
- [76] K. Aydin, I. Bulu, K. Guven, M. Kafesaki, C.M. Soukoulis, E. Ozbay, Investigation of magnetic resonances for different split-ring resonator parameters and designs, *168, New J. Phys.* 7 (Aug. 2005) 168, <https://doi.org/10.1088/1367-2630/7/1/168>.
- [77] H. Elftouh, N.A. Touhami, M. Aghoutane, S. El Amrani, A. Tazon, M. Boussois, Miniaturized microstrip patch antenna with defected ground structure, *PIER C* 55 (2014) 25–33, <https://doi.org/10.2528/PIERC14092302>.
- [78] W. Ali, S. Das, H. Medkour, S. Lakrit, Planar dual-band 27/39 GHz millimeter-wave MIMO antenna for 5G applications, *Microsyst. Technol.* 27 (1) (Jan. 2021) 283–292, <https://doi.org/10.1007/s00542-020-04951-1>.
- [79] M.N. Hasan, S. Bashir, S. Chu, Dual band omnidirectional millimeter wave antenna for 5G communications, *J. Electromagn. Waves Appl.* 33 (12) (2019) 1581–1590, Aug, <https://doi.org/10.1080/09205071.2019.1617790>.
- [80] M.M. Kamal, et al., Infinity shell shaped MIMO antenna array for mm-wave 5G applications, *Electronics* 10 (2) (Jan. 2021) 165, <https://doi.org/10.3390/electronics10020165>.
- [81] K. Raheel, et al., E-shaped H-slotted dual band mmWave antenna for 5G technology, *Electronics* 10 (9) (Apr. 2021) 1019, <https://doi.org/10.3390/electronics10091019>.
- [82] S. Rahman, et al., Nature inspired MIMO antenna system for future mmWave technologies, *Micromachines* 11 (12) (Dec. 2020) 1083, <https://doi.org/10.3390/mi11121083>.
- [83] H.M. Marzouk, M.I. Ahmed, A.-E.H. Shaalan, Novel dual-band 28/38 GHz MIMO antennas for 5G mobile applications, *PIER C* 93 (2019) 103–117, <https://doi.org/10.2528/PIERC19032303>.
- [84] M.I. Khan, et al., A compact mmWave MIMO antenna for future wireless networks, *Electronics* 11 (15) (2022) 2450, <https://doi.org/10.3390/electronics11152450>.
- [85] S. Sharma, M. Arora, A millimeter wave elliptical slot circular patch MIMO antenna for future 5G mobile communication networks, *Progress In Electromagnetics Research M* 110 (13) (2022).
- [86] M.A. Khan, et al., mmWave four-element MIMO antenna for future 5G systems, *Appl. Sci.* 12 (9) (2022) 4280, <https://doi.org/10.3390/app12094280>.
- [87] N. Hussain, W.A. Awan, W. Ali, S.I. Naqvi, A. Zaidi, T.T. Le, Compact wideband patch antenna and its MIMO configuration for 28 GHz applications, *AEU - Int. J. Electron. Commun.* 132 (Apr. 2021) 153612, <https://doi.org/10.1016/j.aue.2021.153612>.
- [88] M. Irshad Khan, M.I. Khattak, S.U. Rahman, A.B. Qazi, A.A. Telba, A. Sebak, Design and investigation of modern UWB-MIMO antenna with optimized isolation, *Apr, Micromachines* 11 (4) (2020) 432, <https://doi.org/10.3390/mi11040432>.
- [89] D.A. Sehrai, et al., A high-gain and wideband MIMO antenna for 5G mm-wave-based IoT communication networks, *Appl. Sci.* 12 (19) (2022) 9530, <https://doi.org/10.3390/app12199530>.
- [90] S.S. Bhatia, N. Sharma, Modified spokes wheel shaped MIMO antenna system for multiband and future 5G applications: design and measurement, *PIER C* 117 (2021) 261–276, <https://doi.org/10.2528/PIERC21111102>.
- [91] B. Aghoutane, S. Das, M. El Ghzaoui, B.T.P. Madhav, H. El Faylali, A novel dual band high gain 4-port millimeter wave MIMO antenna array for 28/37 GHz 5G applications, *AEU - Int. J. Electron. Commun.* 145 (Feb. 2022) 154071, <https://doi.org/10.1016/j.aue.2021.154071>.
- [92] D.A. Sehrai, et al., Compact quad-element high-isolation wideband MIMO antenna for mm-wave applications, *Electronics* 10 (11) (May 2021) 1300, <https://doi.org/10.3390/electronics10111300>.
- [93] T. Addepalli, et al., 8-Port semi-circular arc MIMO antenna with an inverted L-strip loaded connected ground for UWB applications, *Electronics* 10 (12) (Jun. 2021) 1476, <https://doi.org/10.3390/electronics10121476>.
- [94] M. Bilal, S.I. Naqvi, N. Hussain, Y. Amin, N. Kim, High-isolation MIMO antenna for 5G millimeter-wave communication systems, *Electronics* 11 (6) (Mar. 2022) 962, <https://doi.org/10.3390/electronics11060962>.
- [95] A. Patel, et al., Inverted-L shaped wideband MIMO antenna for millimeter-wave 5G applications, *Electronics* 11 (9) (Apr. 2022) 1387, <https://doi.org/10.3390/electronics11091387>.
- [96] R. Janaswamy, D. Schaubert, Analysis of the tapered slot antenna, *IEEE Trans. Antenn. Propag.* 35 (9) (1987) 1058–1065, Sep, <https://doi.org/10.1109/TAP.1987.1144218>.
- [97] M. Ikram, N. Nguyen-Trong, A. Abbosh, Multiband MIMO microwave and millimeter antenna system employing dual-Function tapered slot structure, *IEEE Trans. Antenn. Propag.* 67 (8) (2019) 5705–5710, Aug, <https://doi.org/10.1109/TAP.2019.2922547>.
- [98] E. Al Abbas, M. Ikram, A.T. Mobashsher, A. Abbosh, MIMO antenna system for multi-band millimeter-wave 5G and wideband 4G mobile communications, *IEEE Access* 7 (2019) 181916–181923, <https://doi.org/10.1109/ACCESS.2019.2958897>.
- [99] B.M. Levin, Transparent antennas, *J. Commun. Technol. Electron.* 57 (4) (Apr. 2012) 388–392, <https://doi.org/10.1134/S1064226912040122>.
- [100] K.K. So, B.-J. Chen, C.H. Chan, Microwave and millimeter-wave MIMO antenna using conductive ITO film, *IEEE Access* 8 (2020) 207024–207033, <https://doi.org/10.1109/ACCESS.2020.3037900>.
- [101] A. Desai, C.D. Bui, J. Patel, T. Upadhyaya, G. Byun, T.K. Nguyen, Compact wideband four element optically transparent MIMO antenna for mm-wave 5G applications, *IEEE Access* 8 (2020) 194206–194217, <https://doi.org/10.1109/ACCESS.2020.3033314>.
- [102] I. Nadeem, D.-Y. Choi, Study on mutual coupling reduction technique for MIMO antennas, *IEEE Access* 7 (2019) 563–586, <https://doi.org/10.1109/ACCESS.2018.2885558>.

- [103] M. Alibakhshienari, et al., A comprehensive survey on ‘various decoupling mechanisms with focus on metamaterial and metasurface principles applicable to SAR and MIMO antenna systems, *IEEE Access* 8 (2020) 192965–193004, <https://doi.org/10.1109/ACCESS.2020.3032826>.
- [104] M. Abu, S. A. M. Ali, H. Hassan, and I. M. Ibrahim, “Characterization of artificial magnetic conductor, Electromagnetic Band Gap and Frequency Selective Surface,” vol. 10, no. 2, p. 5.
- [105] S. E. Mendhe and Y. P. Kosta, “METAMATERIAL PROPERTIES AND APPLICATIONS,” p. 6.
- [106] J. Bonache, M. Gil, I. Gil, J. Garcia-Garcia, F. Martin, On the electrical characteristics of complementary metamaterial resonators, *IEEE Microw. Wireless Compon. Lett.* 16 (10) (Oct. 2006) 543–545, <https://doi.org/10.1109/LMWC.2006.882400>.
- [107] N. Hussain, M.-J. Jeong, A. Abbas, N. Kim, Metasurface-based single-layer wideband circularly polarized MIMO antenna for 5G millimeter-wave systems, *IEEE Access* 8 (2020) 130293–130304, <https://doi.org/10.1109/ACCESS.2020.3009380>.
- [108] S.S. Al-Bawri, M.T. Islam, T. Shabbir, G. Muhammad, M.D.S. Islam, H.Y. Wong, Hexagonal shaped near zero index (NZI) metamaterial based MIMO antenna for millimeter-wave application, *IEEE Access* 8 (2020) 181003–181013, <https://doi.org/10.1109/ACCESS.2020.3028377>.
- [109] M. Singh, S. Singh, M.T. Islam, CSRR loaded high gained 28/38GHz printed MIMO patch antenna array for 5G millimeter wave wireless devices, *Microelectron. Eng.* 262 (Jun. 2022) 111829, <https://doi.org/10.1016/j.mee.2022.111829>.
- [110] Md Samsuzzaman, M. Islam, Circularly polarized broadband printed antenna for wireless applications, *Sensors* 18 (12) (Dec. 2018) 4261, <https://doi.org/10.3390/s18124261>.
- [111] X. Shen, Y. Liu, L. Zhao, G.-L. Huang, X. Shi, Q. Huang, A miniaturized microstrip antenna array at 5G millimeter-wave band, *Antennas Wirel. Propag. Lett.* 8 (8) (2019) 1671–1675, Aug, <https://doi.org/10.1109/LAWP.2019.2927460>.
- [112] D.A. Sehrai, et al., Metasurface-based wideband MIMO antenna for 5G millimeter-wave systems, *IEEE Access* 9 (2021) 125348–125357, <https://doi.org/10.1109/ACCESS.2021.3110905>.
- [113] A.A. Ibrahim, W.A.E. Ali, High gain, wideband and low mutual coupling AMC-based millimeter wave MIMO antenna for 5G NR networks, *AEU - Int. J. Electron. Commun.* 142 (Dec. 2021) 153990, <https://doi.org/10.1016/j.aue.2021.153990>.
- [114] S. Tariq, S.I. Naqvi, N. Hussain, Y. Amin, A metasurface-based MIMO antenna for 5G millimeter-wave applications, *IEEE Access* 9 (2021) 51805–51817, <https://doi.org/10.1109/ACCESS.2021.3069185>.
- [115] A.A.R. Saad, H.A. Mohamed, Printed millimeter-wave MIMO-based slot antenna arrays for 5G networks, *AEU - Int. J. Electron. Commun.* 99 (Feb. 2019) 59–69, <https://doi.org/10.1016/j.aue.2018.11.029>.
- [116] Z. Wani, M.P. Abegaonkar, S.K. Koul, Thin planar metasurface lens for millimeter-wave MIMO applications, *IEEE Trans. Antenn. Propag.* 70 (1) (Jan. 2022) 692–696, <https://doi.org/10.1109/TAP.2021.3098571>.
- [117] N. Hussain, M.-J. Jeong, J. Park, N. Kim, A broadband circularly polarized Fabry-perot resonant antenna using A single-layered PRS for 5G MIMO applications, *IEEE Access* 7 (2019) 42897–42907, <https://doi.org/10.1109/ACCESS.2019.2908441>.
- [118] Z. Liu, Fabry-perot resonator antenna, *J. Infrared, Millim. Terahertz Waves* (Dec. 2009), <https://doi.org/10.1007/s10762-009-9605-4>.
- [119] H. Boutayeb, K. Mahdjoubi, A.-C. Tarot, T.A. Denidni, Directivity of an antenna embedded inside a Fabry-Perot cavity: analysis and design, *Microw. Opt. Technol. Lett.* 48 (1) (Jan. 2006) 12–17, <https://doi.org/10.1002/mop.21249>.
- [120] S. Long, M. McAllister, L. Shen, in: *The resonant cylindrical dielectric cavity antenna*, 3, 1983, p. 7.
- [121] S. Keyrouz, D. Caratelli, Dielectric resonator antennas: basic concepts, design guidelines, and recent developments at millimeter-wave frequencies, *Int. J. Antenn. Propag.* 2016 (2016) 1–20, <https://doi.org/10.1155/2016/6075680>.
- [122] L. Zou, D. Abbott, C. Fumeaux, Omnidirectional cylindrical dielectric resonator antenna with dual polarization, *Antennas Wirel. Propag. Lett.* 11 (2012) 515–518, <https://doi.org/10.1109/LAWP.2012.2199277>.
- [123] S. Das, Design of high gain, broadband resonant cavity antenna with meta-material inspired superstrate, *AEU - Int. J. Electron. Commun.* 100 (2019) 39–46.
- [124] Y.M. Pan, X. Qin, Y.X. Sun, S.Y. Zheng, A simple decoupling method for 5G millimeter-wave MIMO dielectric resonator antennas, *IEEE Trans. Antenn. Propag.* 67 (4) (2019) 2224–2234, Apr, <https://doi.org/10.1109/TAP.2019.2891456>.
- [125] Y. Zhang, J.-Y. Deng, M.-J. Li, D. Sun, L.-X. Guo, A MIMO dielectric resonator antenna with improved isolation for 5G mm-wave applications, *Antennas Wirel. Propag. Lett.* 18 (4) (Apr. 2019) 747–751, <https://doi.org/10.1109/LAWP.2019.2901961>.
- [126] N.S. Murthy, Improved isolation metamaterial inspired mm-wave MIMO dielectric resonator antenna for 5G application, *PIER C* 100 (2020) 247–261, <https://doi.org/10.2528/PIERC19112603>.
- [127] A. Iqbal, et al., Electromagnetic bandgap backed millimeter-wave MIMO antenna for wearable applications, *IEEE Access* 7 (2019) 111135–111144, <https://doi.org/10.1109/ACCESS.2019.2933913>.
- [128] S. Kumar, et al., Wideband circularly polarized textile MIMO antenna for wearable applications, *IEEE Access* 9 (2021) 108601–108613, <https://doi.org/10.1109/ACCESS.2021.3101441>.
- [129] S.S. Bukhari, J. Vardaxoglou, W. Whitrow, A metasurfaces review: definitions and applications, *Appl. Sci.* 9 (13) (Jul. 2019) 2727, <https://doi.org/10.3390/app9132727>.
- [130] I.N. Vlasceanu, A. Gharzouni, O. Tantot, M. Lalande, C. Elissalde, S. Rossignol, Geopolymer as dielectric materials for ultra-wideband antenna applications: impact of magnetite addition and humidity, *Open Ceramics* 2 (Jul. 2020) 100013, <https://doi.org/10.1016/j.oceram.2020.100013>.
- [131] K. Trzebiatowski, M. Rzymowski, L. Kulas, K. Nyka, Simple 60 GHz switched beam antenna for 5G millimeter-wave applications, *Antennas Wirel. Propag. Lett.* 20 (1) (Jan. 2021) 38–42, <https://doi.org/10.1109/LAWP.2020.3038260>.
- [132] H. Zahra, M. Hussain, S.I. Naqvi, S.M. Abbas, S. Mukhopadhyay, A simple monopole antenna with a switchable beam for 5G millimeter-wave communication systems, *Electronics* 10 (22) (Nov. 2021) 2870, <https://doi.org/10.3390/electronics10222870>.
- [133] A.G. Alharbi, V. Sorathiya, Ultra-wideband graphene-based micro-sized circular patch-shaped yagi-like MIMO antenna for terahertz wireless communication, *Electronics* 11 (9) (Apr. 2022) 1305, <https://doi.org/10.3390/electronics11091305>.